A&A 653, A151 (2021)
https://doi.org/10.1051/0004-6361/202140830

Astronomy & Astrophysics

Search for candidate strongly lensed dusty galaxies in the *Planck* satellite catalogues

T. Trombetti[1], C. Burigana[1,2,3], M. Bonato[1,4,5], D. Herranz[6,7], G. De Zotti[5], M. Negrello[8], V. Galluzzi[9], and M. Massardi[1,4]

[1] INAF, Istituto di Radioastronomia, Via Piero Gobetti 101, 40129 Bologna, Italy
e-mail: trombetti@ira.inaf.it
[2] Dipartimento di Fisica e Scienze della Terra, Università di Ferrara, Via Giuseppe Saragat 1, 44122 Ferrara, Italy
[3] INFN, Sezione di Bologna, Via Irnerio 46, 40127 Bologna, Italy
[4] INAF, Italian ALMA Regional Centre, Via Piero Gobetti 101, 40129 Bologna, Italy
[5] INAF, Osservatorio Astronomico di Padova, Vicolo dell'Osservatorio 5, 35122 Padova, Italy
[6] Instituto de Física de Cantabria, CSIC-UC, Av. de Los Castros s/n, 39005 Santander, Spain
[7] Departamento de Física Moderna, Universidad de Cantabria, 39005 Santander, Spain
[8] School of Physics and Astronomy, Cardiff University, The Parade, Cardiff CF24 3AA, UK
[9] Osservatorio Astronomico di Trieste, Via G. B. Tiepolo, 11, 34143 Trieste, Italy

Received 18 March 2021 / Accepted 30 July 2021

ABSTRACT

The shallow, all-sky *Planck* surveys at sub-millimetre wavelengths have detected the brightest strongly gravitationally lensed dusty galaxies in the sky. The combination of their extreme gravitational flux-boosting and image-stretching offers the unique possibility of measuring in extraordinary detail the galaxy structure and kinematics in early evolutionary phases through high-resolution imaging and spectroscopic follow-up. This enables us to gain otherwise unaccessible direct information on physical processes in action. However, the extraction of candidate strongly lensed galaxies from *Planck* catalogues is hindered by the fact that they are generally detected with a poor signal-to-noise ratio, except for the few brightest galaxies. Their photometric properties are therefore strongly blurred, which makes them very difficult to single out. We have devised a method capable of increasing the number of identified *Planck*-detected strongly lensed galaxies by a factor of about three to four, although with an unavoidably limited efficiency. Our approach exploits the fact that the sub-millimetre colours of strongly lensed galaxies are definitely colder than those of nearby dusty galaxies, which constitute the overwhelming majority of extragalactic sources detected by *Planck*. The sub-millimetre colours of the 47 confirmed or very likely *Planck*-detected strongly lensed galaxies have been used to estimate the colour range spanned by objects of this type. Moreover, most nearby galaxies and radio sources can be confirmed by cross-matching with the IRAS and PCNT catalogues, respectively. We present samples of lensed candidates selected at 545, 857, and 353 GHz, comprising 177, 97, and 104 sources, respectively. The efficiency of our approach, tested by exploiting data from the SPT survey covering $\simeq$2500 deg^2, is estimated to be in the range 30%−40%. We also discuss stricter selection criteria to increase the estimated efficiency to $\simeq$50%, at the cost of a somewhat lower completeness. Our analysis of SPT data has identified a dozen galaxies that can reliably be considered previously unrecognized *Planck*-detected strongly lensed galaxies. Extrapolating the number of *Planck*-detected confirmed or very likely strongly lensed galaxies found within the SPT and H-ATLAS survey areas, we expect $\simeq$150 to $\simeq$190 such sources over the full $|b| > 20°$ sky.

Key words. gravitational lensing: strong – submillimeter: galaxies – galaxies: high-redshift

1. Introduction

An interesting and unexpected (but see Negrello et al. 2007) result from *Planck* was the detection of ultra-bright strongly lensed sub-millimetre galaxies (SMGs) at high redshift, z, discovered by *Herschel* with extreme magnifications, μ, in the range 10−50 (Herranz et al. 2013; Cañameras et al. 2015; Harrington et al. 2016, 2021; Díaz-Sánchez et al. 2017). These objects offer the unique opportunity to obtain detailed information on the internal structure, gas properties, and kinematics of high-z galaxies during their most active, dust-enshrouded star formation phase (Fu et al. 2012; Nesvadba et al. 2016, 2019; Cañameras et al. 2017a,b, 2018a,b, 2021; Harrington et al. 2018, 2019; Dannerbauer et al. 2019; Planck Collaboration Int. LV 2020).

This information is absolutely crucial for understanding the key processes governing the galaxy formation and early evolution. Current galaxy formation models envisage widely different physical mechanisms that shaped the galaxy properties: mergers, interactions, cold flows from the intergalactic medium, in situ processes (for reviews, see Silk & Mamon 2012; Somerville & Davé 2015). All models have a large number of adjustable parameters that allow them to be consistent with the available statistical information (source counts and redshift distributions).

The only way to obtain direct information on the physical processes at work is to look inside the high-z star-forming galaxies. These are compact, however, with typical effective radii of 1−2 kpc (e.g. Shibuya et al. 2015, 2019; Spilker et al. 2016; Hodge et al. 2016; Ikarashi et al. 2017; Enia et al. 2018; Fujimoto et al. 2018, 2020), corresponding to angular radii of 0.1−0.2 arcsec at $z \simeq 2$−3. Thus they are hardly resolved even by the Atacama Large Millimeter/submillimeter Array (ALMA) or the *Hubble* Space Telescope (HST). If they are resolved, high

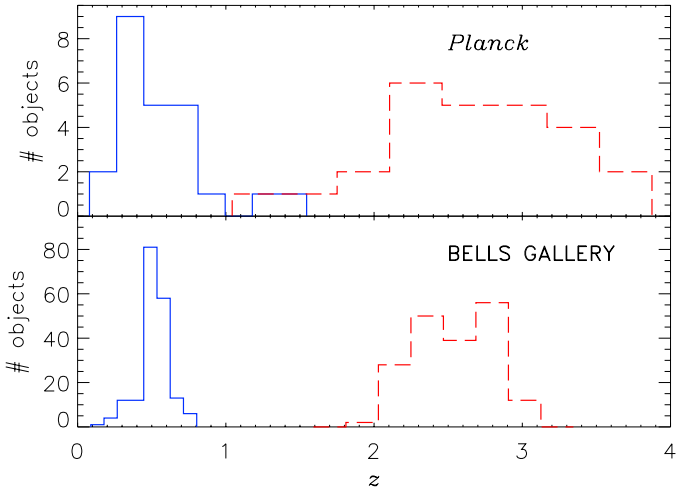

Fig. 1. Redshift distributions of the background-lensed galaxies (solid blue histograms) and of the foreground lenses (dashed red histograms) detected by *Planck* compared with those of the 187 strong gravitational lens candidates in the BELLS GALLERY survey parent sample (Shu et al. 2016).

enough signal-to-noise ratios (S/Ns) per resolution element are achieved only for the brightest galaxies, which are probably not representative of the general population.

Strong gravitational lensing provides a solution of these problems, allowing us to study high-z galaxies in extraordinary detail that are otherwise beyond the reach of present-day instrumentation (e.g. Sun et al. 2021). This is possible thanks to the magnification of the galaxy flux combined with a stretching of images. Because lensing conserves the surface brightness, the effective angular size is stretched by a factor $\mu^{1/2}$ on average.

A spectacular example are ALMA observations with a 0.1″ resolution of the strongly lensed galaxy PLCK_G244.8+54.9 at $z \simeq 3.0$ with $\mu \simeq 30$ (Cañameras et al. 2017b): they reached the astounding spatial resolution of ≃60 pc, which is substantially smaller than the size of Galactic giant molecular clouds. Cañameras et al. (2017b) have also obtained CO spectroscopy, measuring the kinematics of the molecular gas with an uncertainty of 40−50 km s^{-1}. This spectral resolution enables a direct investigation of massive outflows driven by active galactic nuclei (AGN) feedback at high-z, with predicted velocities of ∼1000 km s^{-1} (King & Pounds 2015).

Outflows are advocated by all the main galaxy formation models to explain the star formation inefficiency in galaxies (only ∼10% of the baryons end up in stars). However, the observational confirmation of outflows of the direct fuel for star formation (i.e. molecular gas) is very difficult to achieve at high-z due to the weakness of their spectral signatures (for a review, see Veilleux et al. 2020). Even when outflows are detected, a proper assessment of their properties is limited by the spatial resolution and sensitivity of instruments.

Strong lensing allowed Spilker et al. (2018) and Jones et al. (2019) to detect fast, massive molecular outflows in galaxies at $z = 5.293$ and 5.656, respectively, by means of ALMA spectroscopy. The galaxies were discovered in the South Pole Telescope (SPT) survey. Spilker et al. (2020) found unambiguous evidence for outflows in 8 out of 11 SPT lensed galaxies at $z > 4$.

Prolific searches of strongly lensed galaxies have been carried out in the optical (Cao et al. 2020; Talbot et al. 2021, and references therein). The millimetre (mm) and sub-mm surveys not only complement the optical surveys by extending the selection to dust-enshrouded galaxies, but also reach higher redshifts both of background-lensed galaxies and of foreground lenses, as illustrated by Fig. 1. The mm/sub-mm region is exceptionally well suited to reach high redshifts due to the large, negative K-correction and to the strong cosmological evolution. A further advantage is that lensed SMGs are generally free from blending with foreground lenses and are detected in different wavebands.

Negrello et al. (2007) predicted that essentially all high-z galaxies brighter than $S_{500\,\mu m} = 100$ mJy detected by the *Herschel* surveys would be strongly lensed (magnification $\mu \geq 2$) and pointed out that they might be identified with close to 100% efficiency because the other extragalactic sources above this flux density limit would have been easily recognizable local galaxies plus a small fraction of radio sources. This prediction proved to be accurate, and a total of about 170 candidate strongly lensed galaxies with $S_{500\,\mu m} \geq 100$ mJy have been selected by Negrello et al. (2010, 2017), Wardlow et al. (2013), and Nayyeri et al. (2016) from the *Herschel* Astrophysical Terahertz Large Area Survey (H-ATLAS; Eales et al. 2010), the *Herschel* Multitiered Extragalactic Survey (HerMES; Oliver et al. 2012), and the HerMES Large Mode Survey (HeLMS) plus *Herschel* Stripe 82 Survey (HerS; Viero et al. 2014) catalogues, respectively.

To enlarge the sample of *Herschel*-detected strongly lensed galaxies, it is necessary to investigate at lower flux densities, where these objects are mixed with an increasing fraction of unlensed high-z galaxies. Methods proposed for extracting strongly lensed galaxies exploit the fact that they are located within arcseconds from the galaxy acting as the lens (González-Nuevo et al. 2012, 2019; Bakx et al. 2020). These lens galaxies are close enough to the *Herschel* galaxies to be interpreted as their optical counterparts by likelihood ratio techniques (e.g. Bourne et al. 2016), but they cannot be the sources themselves because they are generally massive ellipticals containing old stellar populations, hence with negligible far-infrared (far-IR) and sub-mm emission.

Planck sub-mm surveys are much shallower that the *Herschel* surveys: their detection limits are higher by more than one order of magnitude. However, the all-sky coverage of the *Planck* mission provided the unique capability of detecting the brightest strongly lensed high-z SMGs in the sky, that is, those that are best suited to deliver high spatial and spectral resolution follow-up data. The shallowness of *Planck* surveys implies that only really extreme magnifications can boost high-z galaxy flux densities above the detection limits. To place the argument in context, we recall that essentially all high-z SMGs brighter than 100 mJy at 600 GHz (500 μm) were found to be strongly lensed (Negrello et al. 2010, 2017; Wardlow et al. 2013; Nayyeri et al. 2016), but the brightest candidate strongly lensed galaxy detected over the 602 deg^2 of the H-ATLAS has a flux density of 465.7 mJy at 857 GHz (Negrello et al. 2017). For comparison, the 90% completeness limit at this frequency of the second *Planck* Catalogue of Compact Sources (PCCS2; Planck Collaboration XXVI 2016) in the so-called extragalactic zone is of 791 mJy. Correspondingly, the estimated gravitational magnifications of *Planck*-detected lensed galaxies, mostly in the range 10−50 (Cañameras et al. 2015; Harrington et al. 2021), are substantially higher than those of H-ATLAS lensed galaxies, which are in the range ∼5−15 (Negrello et al. 2017; Enia et al. 2018). The unique possibilities offered by the *Planck* selection are clear.

Searching the literature, we have collected a total of 27 *Planck*-detected strongly lensed galaxies (Table 1). All but two

Table 1. Confirmed strongly lensed galaxies detected by *Planck*.

Planck name	RA (deg)	Dec (deg)	S_{353}	S_{545}	S_{857}	z	z_l	Ref.
P353 G293.74–69.76	17.4580	−47.0360	273 ± 49	–	741 ± 132	3.614	0.669	S16, R20
P545 G190.40–83.77	19.1949	−24.6172	–	684 ± 102	1138 ± 132	2.1245	0.4	H20
P545 G287.12–68.67	21.2800	−47.3987	226 ± 46	517 ± 79	903 ± 113	2.5148	0.305	W13
P545 G160.59–56.77	32.4210	0.2626	329 ± 66	813 ± 109	1309 ± 165	2.5534	0.202	H16
PE857 G149.41–34.16	36.6416	23.7579	498 ± 78	1174 ± 126	2263 ± 250	3.1190	0.34	H20
P857 G227.77–60.61	46.2943	−30.6084	–	–	613 ± 101	2.2624	0.1–0.5	H20
P545 G157.43+30.34	117.2155	59.6982	407 ± 67	927 ± 108	–	2.7544	0.402	H20
P545 G211.62+32.22	131.7090	15.0965	431 ± 58	1114 ± 89	1660 ± 117	2.6615	0.1	H20
PHz G200.61+46.09	143.0985	27.4167	370 ± 190	586 ± 68	747 ± 78	≃3.0	0.6	C15
P545 G145.25+50.84	163.3439	60.8635	450 ± 50	782 ± 90	–	3.6000	–	C15
P545 G244.76+54.94	163.4710	5.9392	444 ± 49	915 ± 91	1334 ± 131	3.0055	1.525	C15, H20
P857 G158.56+64.72	171.8060	46.1567	–	–	886 ± 128	1.3036	0.415	H20
P857 G188.25+73.11	174.5230	32.9658	–	–	882 ± 145	2.0183	0.6	H20
P545 G231.27+72.22	174.8406	20.4147	–	533 ± 85	–	2.8584	0.57	C15, H20
P353 G270.57+58.50	176.6579	−0.1922	287 ± 50	–	956 ± 148	3.2592	1.2247	F12, He13, N17
P545 G138.59+62.02	180.5320	53.5778	–	633 ± 77	835 ± 106	2.4416	0.212	H16
P353 G076.26+79.96	201.6254	33.7353	255 ± 49	–	–	2.9507	0.7856	N17
P545 G007.97+80.28	202.3920	22.7242	283 ± 56	921 ± 97	1612 ± 121	2.0401	0.443	D17
P545 G104.43+66.26	204.1456	49.2204	–	539 ± 80	852 ± 126	3.2548	0.28	H20
P857 G052.27+77.90	206.1225	30.5094	–	–	705 ± 130	2.3010	0.6721	N17
P857 G030.03+62.79	222.4941	22.6436	–	–	703 ± 125	2.1536	–	H20
P545 G045.11+61.10	225.6502	29.3475	333 ± 64	498 ± 86	–	3.4270	0.56	C15, Ne16
P545 G080.25+49.86	236.1350	50.3961	–	504 ± 77	–	2.5988	0.673	C15, H20
P857 G107.64+36.93	241.8242	73.7842	–	–	761 ± 104	1.4839	0.65	H16, H20
P545 G092.49+42.89	242.3240	60.7558	307 ± 45	788 ± 79	1240 ± 113	3.2555	0.45	H16, H20
P545 G053.44–36.27	323.7983	−1.0478	337 ± 57	775 ± 109	947 ± 165	2.3259	0.325	Sw10
P353 G325.97–59.46	353.0972	−53.9804	307 ± 52	–	–	2.73	–	Su21

Notes. Flux densities are in mJy. They are taken from the PCCS2 catalogue except for the source at RA = 36.6416 deg, Dec = 23.7579 deg, which is in the PCCS2E catalogue (sources of unknown reliability) and for that at RA = 143.0985 deg, Dec = 27.4167 deg, which is one of the *Planck* high-z source candidates (PHz catalogue; Planck Collaboration Int. XXXIX 2016). The redshifts of the source and of the lens are denoted by z and z_l, respectively. In the first column, P stands for PCCS2, PE for PCCS2E, and the adjacent number is the selection frequency (GHz).
References. C15, Cañameras et al. (2015); D17, Díaz-Sánchez et al. (2017); F12, Fu et al. (2012); H16, Harrington et al. (2016); H20, Harrington et al. (2021); He13, Herranz et al. (2013); N17, Negrello et al. (2017); Ne16, Nesvadba et al. (2016); R20, Reuter et al. (2020); S16, Spilker et al. (2016); Su21, Sun et al. (2021); Sw10, Swinbank et al. (2010); W13, Weiß et al. (2013).

of them are listed in the Second *Planck* Catalogue of Compact Sources (PCCS2; Planck Collaboration XXVI 2016), one in the PCCS2E, which contains sources with unknown reliability, and one in the catalogue of *Planck* high-z source candidates, detected in the cleanest 26% of the sky (PHz catalogue; Planck Collaboration Int. XXXIX 2016).

Cañameras et al. (2015) listed three more sources as *Planck*-detected (at right ascension and declination (RA, Dec) in deg: 139.619, 51.7064; 171.8108, 42.4736; 217.3249, 59.3525). Another four sources were listed by Harrington et al. (2016) and/or Harrington et al. (2021) at 200.5730, 9.3907; 200.7615, 55.6003; 217.0995, 35.4389; 348.4860, and 1.1549. None of them appears in the last versions of the online *Planck* catalogues.

The measured redshifts are in the range 1.3−3.6, implying that a statistically well-defined sample of *Planck*-lensed galaxies would be very well suited for investigating the structure of galaxies across the peak of the cosmic star formation rate. However, searches have been fragmentary so far and were conducted over limited sky areas, implying that the available sample is highly inhomogeneous and incomplete.

Finding the rare *Planck*-detected strongly lensed galaxies among the several thousand local dusty galaxies is difficult, however. Statistical selection techniques such as those successfully used to select *Herschel*-detected strongly lensed candidates fainter than $S_{500\,\mu m}$ = 100 mJy (González-Nuevo et al. 2012, 2019; Bakx et al. 2020), mentioned above, cannot be applied: the typical rms positional error of the relevant sources, computed using Eq. (7) of Planck Collaboration XXVI (2016), is 1.5 arcmin, which is a factor of 26 larger than the typical positional error (3.4 arcsec; Bourne et al. 2016) for sources observed with the *Herschel*–Spectral and Photometric Imaging Receiver (SPIRE).

To search for counterparts to H-ATLAS sources, Bourne et al. (2016) considered Sloan Digital Sky Survey (SDSS) galaxies with $r_{\rm model} < 22.4$. Their surface density is $\simeq 1.2 \times 10^4\,{\rm deg}^{-2}$, so that within the 2σ search radius of 3 arcmin, there are ≃94 SDSS galaxies on average. Similarly, the surface density of Wide-Field Infrared Survey Explorer (WISE) galaxies is $\simeq 9.9 \times 10^3\,{\rm deg}^{-2}$ (Jarrett et al. 2017), so that there are ≃80 WISE galaxies within a 3 arcmin radius on average. For comparison, the number of chance associations within 10″, the search radius generally used in the *Herschel* case, is ≃0.09 (SDSS) or ≃0.08 (WISE). We did not find any valid criterion to identify plausible foreground lenses among the many dozen galaxies lying within the *Planck* search radius.

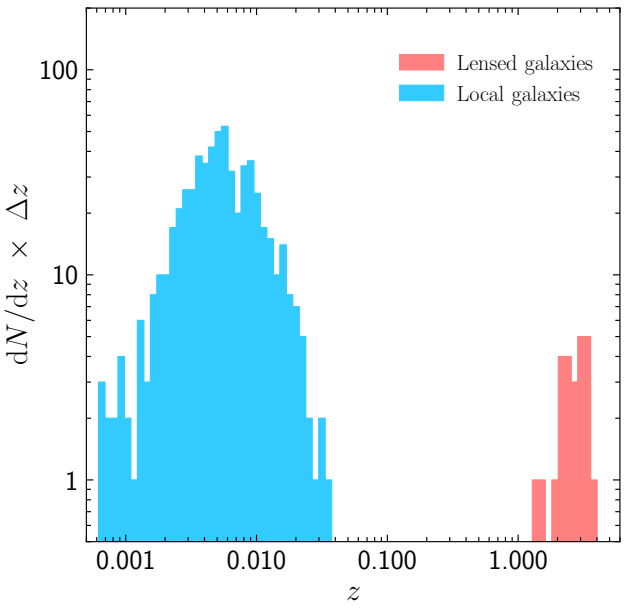

Fig. 2. Redshift distribution of *Planck* Early Release Compact Source Catalogue (ERCSC; Planck Collaboration VII 2011) galaxies detected at 545 GHz (Negrello et al. 2013, no more recent redshift distribution for a complete sample of *Planck* dusty galaxies is available). They are all local ($z < 0.1$). At fainter flux densities, strongly lensed galaxies at much higher redshifts ($z \gtrsim 1$) begin to appear, with nothing in between. The redshift distribution of known strongly lensed galaxies detected by *Planck* (Table 1) is shown here. The broad gap between the two populations persists at least down to a flux density of 100 mJy at 600 GHz (Negrello et al. 2017).

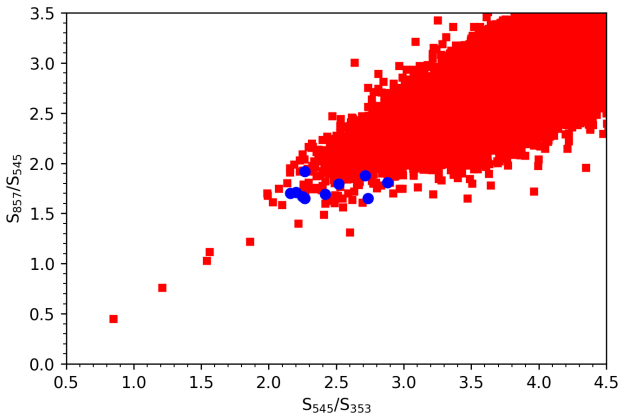

Fig. 3. Distribution in the S_{857}/S_{545} vs S_{545}/S_{353} colour–colour plot of *Planck*-detected galaxies with $S_{545} \geq 500$ mJy. For this diagram we used the multi-band BeeP photometry (Planck Collaboration Int. LV 2020). Radio sources were removed by cross-matching the sample with the PCNT catalogue (Planck Collaboration Int. LIV 2018). The ten confirmed strongly lensed galaxies in this sample (filled blue circles) have colours at the red end of the distribution of the other galaxies (filled red squares). Still redder objects are likely GCC (see text).

Another possibility would be to use machine-learning techniques to select lensed candidates. This would require massive simulations using the *Planck* Sky Model (Delabrouille et al. 2013), for instance, to produce a tailored training set. However, we preferred to resort to the work-intensive approach described in Sect. 2, where we also present our results. In Sect. 3 we summarise and discuss our main conclusions.

2. Method

2.1. Overview

As mentioned above, picking up strongly lensed galaxies from *Planck* catalogues is difficult because they are a tiny fraction of the detected sources and their flux densities are generally near the detection limit, as expected given the steepness of the bright end of their source counts (Perrotta et al. 2002, 2003; Negrello et al. 2007, 2017; Vieira et al. 2010; Mocanu et al. 2013; Everett et al. 2020). Sub-mm PCCS2 sources at high Galactic latitude ($|b| > 20°$)[1] are mostly nearby star-forming galaxies with a small fraction of extragalactic radio sources, which dominate at cm and mm wavelengths (Planck Collaboration Int. VII 2013). In addition, there are galaxy over-densities (Planck Collaboration Int. XXVII 2015; Planck Collaboration Int. XXXIX 2016), Galactic cirrus (Herranz et al. 2013) and Galactic cold clumps (GCC; Planck Collaboration XXVIII 2016), intensity peaks of the cosmic infrared background (CIB), and the rare strongly lensed galaxies we searched for.

Because we are interested in dusty galaxies, we considered only *Planck* channels at $\nu \geq 353$ GHz. As predicted by Negrello et al. (2007) and confirmed by the analysis of H-ATLAS data (Negrello et al. 2017), unlensed dusty galaxies are at $z \lesssim 0.1$ (see also Negrello et al. 2013) and lensed galaxies are at $z > 1$ (see Fig. 2) at the bright detection limits of the *Planck* sub-mm surveys. They therefore have substantially colder sub-mm colours.

Thus sub-mm colours are a distinctive property of strongly lensed galaxies. The question then is whether these sources can be selected simply based on colours. The PCCS2 photometry is frequently limited to one or two frequencies, which is not enough to answer this question. Fortunately, multi-band photometry obtained with the Bayesian extraction and estimation package (BeeP) has recently been published (Planck Collaboration Int. LV 2020). We selected sources with $S_{545} \geq 500$ mJy at high Galactic latitudes ($|b| \geq 20°$). This flux density limit is slightly lower than the 90% completeness limit in the extragalactic zone given by Planck Collaboration XXVI (2016), 555 mJy, but consistent with the limit obtained from the comparison between *Planck* and H-ATLAS photometry (Maddox et al. 2018).

Radio sources were identified and removed by cross-matching the BeeP sample with the *Planck* multi-frequency catalogue of non-thermal sources (PCNT; Planck Collaboration Int. LIV 2018). The distribution of sources in the S_{857}/S_{545} vs S_{545}/S_{353} plane is shown in Fig. 3. The ten confirmed strongly lensed galaxies comprised in the BeeP sample populate the red end of the distribution, but their positions in the diagram are not clearly separated from those of unlensed galaxies. This shows that colours are useful to remove most nearby galaxies, but these are still by far more numerous than lensed galaxies in any region encompassing the colours of the latter. The reason is that the uncertainties in the flux densities measured by *Planck* are so large that the differences in colour between local and lensed galaxies are blurred. Thus the selection must be refined.

[1] At low Galactic latitudes the reliability of source detection cannot be accurately assessed because of the confusion from Galactic cirrus emission. Therefore the Planck Collaboration has adopted a set of Galactic masks, defined by Planck Collaboration XV (2014), to exclude regions to various levels of dust contamination. Our choice, $|b| > 20°$, roughly corresponds to the region outside the *Planck* G65 mask.

Figure 3 also shows that there are objects with colours even redder than those of strongly lensed galaxies. Two out of the five objects with the reddest colours (those at RA = 83.9031 deg, Dec = 22.012 deg; RA = 142.4874 deg, Dec = −23.2730 deg, with $S_{857}/S_{545} = 0.76$, $S_{545}/S_{353} = 1.21$ and $S_{857}/S_{545} = 1.12$, $S_{545}/S_{353} = 1.56$, respectively) are listed in the *Planck* catalogue of GCC (Planck Collaboration XXVIII 2016). The other 3 (170.8088, −48.6199; 277.4627, 1.4644; 343.5329, 16.1255 with $S_{857}/S_{545} = 1.22$, $S_{545}/S_{353} = 1.86$; $S_{857}/S_{545} = 1.03$, $S_{545}/S_{353} = 1.54$ and $S_{857}/S_{545} = 0.45$, $S_{545}/S_{353} = 0.84$, respectively) are also likely GCC, although the data do not yet allow a firm classification.

The BeeP catalogue contains only sources listed in the PCCS2+2E at 857 GHz. It misses some of the reddest sources that are detected at lower frequencies, including most of the known *Planck*-detected strongly lensed galaxies. To achieve a comprehensive selection of strongly lensed candidates, we therefore need to revisit the PCCS2 catalogues at 353 and 545 GHz. Again, we confined ourselves to sources at $|b| \geq 20°$, but to be as inclusive as possible, we did not impose any flux-density cut. We adopted the *Planck* DETFLUX photometry because of its sensitivity is higher than that of APERFLUX, although the latter is more robust at ≥353 GHz (Planck Collaboration XXVI 2016). Using DETFLUX, our selection criteria, specified in the subsections below, recover more confirmed strongly lensed galaxies than using APERFLUX. For example, at 545 GHz, we recover 18 confirmed strongly lensed galaxies, while only 11 are recovered using APERFLUX. The reason is that APERFLUX yields substantially lower S/Ns for our faint sources. Moreover, their colours are spread throughout the region that is occupied by local dusty galaxies. This shows that selection criteria based on colours are much less efficient: it is crucial for our purposes to reach deeper.

A first cleaning of the initial $|b| \geq 20°$ samples at each frequency was obtained by cross-matching them with the Infrared Astronomical Satellite (IRAS) PSC/FSC[2] Combined Catalogue (Abrahamyan et al. 2015) using a 3 arcmin search radius. Because the dust emission spectrum of low-z galaxies generally peaks in the range 60−150 μm (Lagache et al. 2005), that is, within or close to the IRAS wavelength range, IRAS is substantially more sensitive to these objects than *Planck*. Not all IRAS galaxies are at low z. About 4% are at $z > 0.3$, and a small fraction (0.7%) are hyper-luminous infrared galaxies and dusty quasars at z of up to ≃4, including 4 strongly lensed galaxies (Rowan-Robinson et al. 2018). However, none of the IRAS galaxies with extreme infrared (IR) luminosities, listed in Table 5 of Rowan-Robinson et al. (2018), has a PCCS2 counterpart. By dropping PCCS2 sources with IRAS counterparts, we thus rid the sample of nearby dusty galaxies without affecting high-z objects.

The removal of radio sources is slightly less straightforward. Matches with the PCNT include dusty galaxies hosting radio nuclei. Because their sub-mm colours are dominated by dust emission, they should be dealt with as the other dusty galaxies. We therefore inspected the matches one by one and verified whether after subtracting the radio contribution extrapolated from lower frequencies, the sub-mm colours were consistent with dust emission, that is, the continuum spectra showed a steepening from mm to sub-mm wavelengths. Objects with spectra consistent with being dust-dominated at sub-mm wavelengths were kept. At first we thought that sources with counterparts in the *Planck* GCC catalogue should be removed, but we found that the GCCs included 8 confirmed strongly lensed galaxies and therefore refrained from removing GCC sources. This is even expected. Although Planck Collaboration XXVIII (2016) applied three independent methods for removing extragalactic sources from their sample, they were unable to identify strongly lensed galaxies, whose colours are similar to those of the GCCs.

To clean the samples further, we made a selection based on sub-mm colours. The obvious benchmark for this purpose is the sample of confirmed strongly lensed *Planck*-detected galaxies (Table 1). Because the number of these objects is limited, we complemented it with other *Planck* galaxies whose properties indicate that they are very likely strongly lensed.

Negrello et al. (in prep.) carried out observations of a preliminary sample of candidate strongly lensed galaxies with $S_{545} \geq 500$ mJy using the Submillimeter Common-User Bolometer Array 2 (SCUBA-2), and detected 12 of them. The SCUBA-2 detection implies that these objects are point-like, that is, they are not cold extended objects like cold clumps, proto-clusters of high-z dusty galaxies, or positive fluctuations of the CIB. Their red colours imply substantial redshifts, but galaxies at substantial redshifts are almost certainly strongly lensed. This point is illustrated by Fig. 2, which shows a striking bimodality in the redshift distribution of *Planck*-detected galaxies. On the one hand, we have nearby late-type galaxies at $z \lesssim 0.1$, which are easily recognizable in optical/near-infrared catalogues. On the other hand, we have dust enshrouded and therefore optically very faint, gravitationally lensed galaxies at $z \gtrsim 1$. The bimodality is inherent in shallow sub-mm surveys and was shown to persist down to detection limits much deeper than that of *Planck*; it is seen in *Herschel* surveys for $S_{\rm lim,600} = 100$ mJy (Negrello et al. 2017). *Planck*-detected galaxies at $z > 0.2$ would be hyperluminous infrared galaxies (HyLIRGs, $L_{\rm IR} > 10^{13}\,L_{\odot}$). HyLIRGs are not detected at redshifts of a few tenths (Gruppioni et al. 2013); if they were present, they would have been detected by IRAS (Rowan-Robinson et al. 2018). On the other hand, the probability that SMGs undergo strong lensing is heavily suppressed at $z \lesssim 1$ (Perrotta et al. 2002; Negrello et al. 2007; Hezaveh & Holder 2011). Only at higher redshifts there are enough very luminous IR galaxies and the optical depth for strong gravitational lensing is large enough to yield the extreme amplifications needed to make galaxies detectable by *Planck* (to reach the *Planck* detection limits, galaxies must be both intrinsically ultra-luminous and very highly magnified). Three of the 12 sources detected by Negrello et al. (in prep.) with SCUBA-2 were later confirmed by Harrington et al. (2021) to be strongly lensed.

Furthermore, a cross-match of galaxies detected by *Planck* with the catalogues of SPT galaxies (Everett et al. 2020) yielded four more sources with redshifts indicative of strong lensing. Finally, we added the seven galaxies that are listed as *Planck*-detected by either Cañameras et al. (2015) or Harrington et al. (2016, 2021), which are not listed in the PCCS2, but are present in earlier versions of the *Planck* point source catalogues.

Most of these 47 sources do not have PCCS2 photometry at all three frequencies of interest (353, 545, and 857 GHz), as necessary to determine their sub-mm colours. To obtain uniform photometry for the full sample, we performed a multi-frequency analysis with the matrix multi-filter method described by Planck Collaboration Int. LIV (2018). This technique allowed us to derive flux density estimates or upper limits at all frequencies of interest and also to improve the S/N at the frequencies for which PCCS2 flux densities are available.

[2] Point Source and Faint Source catalogues (PSC and FSC, respectively).

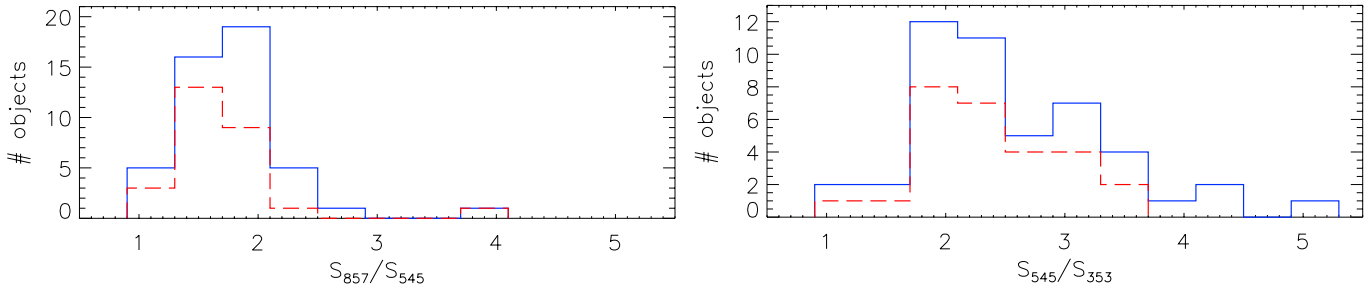

Fig. 4. Distributions of sub-mm colours S_{857}/S_{545} and S_{545}/S_{353} of the 47 confirmed plus very likely *Planck*-detected strongly lensed galaxies (solid blue histograms). The dashed red histograms show the distributions of the 27 confirmed strongly lensed galaxies only.

We note in passing that there are significant differences between the BeeP and the matched matrix filters (MTXF) photometry. The BeeP photometry is based on the all-sky temperature maps at 353, 545, and 857 GHz from the *Planck* 2015 release (PR2; Planck Collaboration I 2016), which was also the source for the PCCS2 photometry. The Beep catalogue provides two sets of flux-density estimates based on different models for the spectral energy distribution (SED): the modified blackbody (MBB), and the free model. The two sets agree well. We chose the MBB flux densities, which seem to benefit from a better background subtraction.

The MTXF photometry instead exploits the most recent publicly available release (PR3; Planck Collaboration I 2020) in the *Planck* Legacy Archive. However, we confirmed that using PR2 maps, we obtain very minor differences, ≃2%. Much larger differences are produced by the different methods for measuring source flux densities. The BeeP photometry agrees well with the PCCS2 APERFLUX but not with DETFLUX. For example, at 857 GHz, the DETFLUX values are lower by ∼24% on average than the BeeP values. Hence the BeeP photometry is close to aperture photometry.

In its current implementation, the MTXF method instead assumes that sources are point-like, that is, that their spatial profile is that of the instrumental beam. It is therefore closer to DETFLUX and works well for the high-z sources we are interested in. On the other hand, it is bound to underestimate the flux density of extended sources such as nearby dusty galaxies. This is indeed what we see. The ratio of the MTXF and BeeP flux densities is lower for the brightest sources, which are very nearby dusty galaxies. The mean MTXF/BeeP ratios for the 388 common sources in the parent sample are 0.78, 0.75, and 0.84 at 857, 545, and 353 GHz, respectively, which is close to the mean ratios between DETFLUX and BeeP flux densities. However, the ratios approach unity if we restrict ourselves to the weaker sources of interest here.

Another factor that may affect flux density estimates is positional accuracy. There are some differences between the positions at which MTXF and BeeP locate the sources. Planck Collaboration Int. LV (2020) argued that positional offsets can account for a difference of up to 5% between BeeP and PCSS2 APERFLUX.

The MTXF photometry at $\nu \geq 217$ GHz of confirmed strongly lensed galaxies in Table 1 is presented in Table 2. The distributions of the S_{857}/S_{545} and S_{545}/S_{353} flux density ratios of all the 47 confirmed or very likely strongly lensed galaxies are shown in Fig. 4. All sources but one have $S_{857}/S_{545} < 2.75$. The highest S_{857}/S_{545} ratio is very uncertain because the source has a low S/N at 545 GHz ($S/N_{545} \simeq 1.5$): it has an rms error of 74%, and the central value of the ratio is higher than 2.75 by only 0.36σ.

The distribution of S_{545}/S_{353} ratios is substantially broader and more uncertain. This is because the S/N is generally low at 353 GHz: about one-third of the sources have $S/N_{353} < 3$ and only 11 have $S/N_{353} > 5$. Thus this ratio did not help much with the selection, and we ignored it. We did not impose any lower limit to the S_{857}/S_{545} ratio because sources with low values may be at higher redshifts than confirmed strongly lensed galaxies in our sample and thus is particularly interesting.

The application of the MTXF technique is quite demanding in terms of computer time. It is therefore not practical to apply it to all sources detected by *Planck* at frequencies ≥353 GHz. We therefore chose to first clean the 353 and 545 GHz samples as far as possible, exploit the available information, and to obtain the MTXF photometry for the cleaned samples alone. At 857 GHz we used the BeeP photometry. Our procedure for selecting *Planck*-detected strongly lensed galaxies is summarised in the flowchart of Fig. 5.

2.2. Selection at 545 GHz

As mentioned above, we adopted 545 GHz as our reference frequency. This frequency is expected to maximize the ratio between the number of lensed and unlensed galaxies (although this ratio is nevertheless extremely low) because compared to the 857 GHz selection, it favours redder sources while being more sensitive to dusty galaxies than the 353 GHz channel.

After removing IRAS galaxies and radio sources, we were left with 556 sources. These constitute our parent sample. Applying the $S_{857}/S_{545} < 2.75$ criterion to the MTXF photometry of the parent sample, we obtained a sample of 202 candidate strongly lensed galaxies. A check made using the National Aeronautics and Space Administration/Infrared Processing and Analysis Center (NASA/IPAC) Extragalactic Database (NED) showed that some of these sources are associated with nearby galaxies that escaped rejection based on the cross-match with the IRAS catalogue. With the help of the Aladin Sky Atlas (Bonnarel et al. 2000; Boch & Fernique 2014), we selected 25 such sources that were removed from the sample. This left the 177 candidates that are listed in Table A.1.

We also considered a stricter criterion, $S_{857}/S_{545} < 2.35$. Only 3 confirmed or very likely strongly lensed sources exceed this limit, and for 2 of them, the ratio is quite uncertain. We found 116 sources that meet this criterion. The check on the NED showed that 5 of them are local galaxies, which left 111 sources with $S_{857}/S_{545} < 2.35$ (see Table A.1).

A test of the efficiency of our selection of strongly lensed candidates was carried out by singling out sources within the SPT area, that is, $-65° \leq$ Dec $\leq -40°$ and RA between 20 h and 7 h (Everett et al. 2020). In this area lie 15 sources with $S_{857}/S_{545} < 2.75$, 8 of which have an STP counterpart

Table 2. MTXF photometry of confirmed strongly lensed galaxies listed in Table 1.

RA	Dec	S_{217}	S_{353}	S_{545}	S_{857}	S/N_{217}	S/N_{353}	S/N_{545}	S/N_{857}	S_{857}/S_{545}	S_{545}/S_{353}	S_{353}/S_{217}
17.4579	−47.0363	81 ± 25	248 ± 72	530 ± 105	854 ± 187	3.2	3.5	5.1	4.6	1.61	2.14	3.06
19.1952	−24.6171	58 ± 27	264 ± 67	650 ± 111	1351 ± 260	2.1	3.9	5.9	5.2	2.08	2.46	4.58
21.2802	−47.3991	83 ± 30	271 ± 53	618 ± 102	1078 ± 162	2.8	5.1	6.1	6.7	1.74	2.28	3.26
32.4206	0.2624	139 ± 35	459 ± 91	885 ± 133	1384 ± 240	4.0	5.0	6.6	5.8	1.56	1.93	3.31
36.6414	23.7581	103 ± 36	424 ± 100	1320 ± 163	2481 ± 413	2.8	4.2	8.1	6.0	1.88	3.11	4.12
46.2946	−30.6084	36 ± 31	134 ± 77	415 ± 98	694 ± 163	1.2	1.8	4.2	4.2	1.67	3.09	3.76
117.2154	59.6986	48 ± 36	465 ± 70	819 ± 109	1141 ± 250	1.3	6.6	7.5	4.6	1.39	1.76	9.71
131.7091	15.0964	101 ± 36	494 ± 80	1387 ± 100	2347 ± 190	2.8	6.1	13.9	12.3	1.69	2.81	4.89
143.0986	27.4164	143 ± 36	328 ± 78	531 ± 97	672 ± 188	4.0	4.2	5.5	3.6	1.27	1.62	2.30
163.3439	60.8635	139 ± 31	505 ± 64	862 ± 114	1032 ± 215	4.4	7.9	7.6	4.8	1.20	1.71	3.62
163.4709	5.9392	62 ± 29	370 ± 64	1027 ± 108	1852 ± 197	2.1	5.7	9.5	9.4	1.80	2.77	6.02
171.8062	46.1568	88 ± 27	81 ± 55	142 ± 95	529 ± 161	3.3	1.5	1.5	3.3	3.73	1.75	0.92
174.5231	32.9658	44 ± 29	123 ± 62	388 ± 112	822 ± 191	1.5	2.0	3.5	4.3	2.12	3.17	2.78
174.8401	20.4146	90 ± 29	222 ± 68	505 ± 94	585 ± 169	3.1	3.3	5.3	3.5	1.16	2.27	2.46
176.6581	−0.1923	61 ± 29	318 ± 60	601 ± 113	1026 ± 179	2.1	5.3	5.3	5.7	1.71	1.89	5.21
180.5322	53.5779	42 ± 27	168 ± 63	544 ± 94	909 ± 152	1.6	2.7	5.8	6.0	1.67	3.24	3.96
201.6254	33.7353	47 ± 27	308 ± 66	344 ± 101	518 ± 181	1.7	4.7	3.4	2.9	1.50	1.12	6.62
202.3920	22.7242	73 ± 31	247 ± 70	886 ± 106	1687 ± 183	2.4	3.5	8.3	9.2	1.90	3.59	3.38
204.1455	49.2205	50 ± 26	240 ± 59	537 ± 95	946 ± 176	1.9	4.1	5.7	5.4	1.76	2.24	4.79
206.1225	30.5094	40 ± 31	131 ± 73	376 ± 98	631 ± 169	1.3	1.8	3.8	3.7	1.68	2.87	3.24
222.4941	22.6436	59 ± 37	274 ± 97	543 ± 106	912 ± 184	1.6	2.8	5.1	4.9	1.68	1.98	4.66
225.6502	29.3475	72 ± 29	332 ± 70	608 ± 95	829 ± 169	2.5	4.8	6.4	4.9	1.37	1.83	4.59
236.1350	50.3961	94 ± 27	220 ± 49	488 ± 92	723 ± 153	3.5	4.5	5.3	4.7	1.48	2.22	2.34
241.8239	73.7844	25 ± 21	132 ± 47	459 ± 91	951 ± 160	1.2	2.8	5.0	6.0	2.07	3.48	5.25
242.3240	60.7558	29 ± 23	296 ± 44	800 ± 84	1508 ± 162	1.2	6.7	9.5	9.3	1.88	2.70	10.30
323.7983	−1.0478	85 ± 34	396 ± 78	835 ± 122	1154 ± 224	2.5	5.1	6.8	5.1	1.38	2.11	4.68
353.0980	−53.9802	686 ± 27	290 ± 60	542 ± 120	725 ± 229	2.5	4.8	4.5	3.2	1.34	1.87	4.29

Notes. Flux densities and errors are in mJy, rounded to 1 mJy. Equatorial coordinates, RA and Dec, J2000, are in degrees. S/N is the signal-to-noise ratio at the frequency in the subscript.

within 3 arcmin; the latter include 1 confirmed and 4 very likely strongly lensed galaxies. The other 3 SPT matches are classified by Everett et al. (2020) as dusty unresolved sources and do not have any counterpart in the local universe. They might therefore well be high-z strongly lensed galaxies. In this case, our selection efficiency would be ∼50%. One of the 7 sources lacking an SPT counterpart (at RA = 77.30626, Dec = −55.17907) is a PHz source at $z_{\rm phot}$ = 2.61 (Planck Collaboration Int. XXXIX 2016). It might be a proto-cluster of dusty galaxies. The other 6 sources might be cirrus, although other possibilities cannot be ruled out.

The 177 sources with $S_{857}/S_{545} < 2.75$ include 13 matches with PHz objects, all with $S_{857}/S_{545} < 1.9$, and 20 matches with GCCs (Planck Collaboration XXVIII 2016). Seven of the PHz matches and also 7 of the GCC matches are confirmed strongly lensed galaxies (see the last column of Table A.1).

There are also 7 matches with *Planck* SZ clusters within 5 arcmin[3]. Studies of the strong-lensing statistics have shown that galaxy clusters contribute substantially to the probability distribution at the very high magnifications typical of *Planck*-detected lensed galaxies (Hilbert et al. 2008; Lima et al. 2010; Robertson et al. 2020). Three of the confirmed strongly lensed galaxies (at RA, Dec 117.2155, 59.6982; 163.3440, 60.8636; and 323.7983, −1.0478) are associated with clusters detected by *Planck* through the Sunyaev-Zeldovich (SZ) effect (Planck Collaboration XXVII 2016). A cross-match of the full catalogue of PCCS2 detections at 545 GHz with the *Planck* SZ catalogue did not yield any other association within 5′, except for the chance alignment of the nearby bright galaxy NGC 4523, which is the obvious identification of the *Planck* source.

We also cross-matched our candidates with other large catalogues of confirmed galaxy clusters, namely the Massive and Distant Clusters of WISE Survey (MaDCoWS; Gonzalez et al. 2019), the COnstraining Dark Energy with X-ray (CODEX) clusters (Finoguenov et al. 2020), the Meta-Catalogue of X-ray detected Clusters of galaxies (MCXC; Piffaretti et al. 2011), and the catalogues of clusters detected through the SZ effect by the SPT (Bleem et al. 2015) and by the Atacama Cosmology Telescope (ACT; Hilton et al. 2021) surveys. We found 13 matches of our candidate strongly lensed galaxies with clusters in at least one of these catalogues. These source have a "C" label in the last column of Table A.1. A more complete analysis of the associations of our lensed candidates with galaxy clusters will be possible when the eROSITA (extended ROentgen Survey with an Imaging Telescope Array) catalogue, expected to contain ∼10^5 galaxy clusters (Merloni et al. 2012), will be available.

Restricting ourselves to $S_{857}/S_{545} < 2.35$, we have 12 sources in the SPT area, with the same 8 matches with SPT sources. This corresponds to a success rate of 5 out of 12 (taking into account only the 5 confirmed or very likely strongly lensed) to 2 out of 3, in the case that all the 8 matches are strongly lensed. The numbers of matches with PHz sources and SZ clusters remain the same, the matches with GCCs decrease to 13.

2.3. Selection at 857 GHz

As shown in Table 1 some confirmed strongly lensed galaxies were detected by *Planck* only at 857 GHz. The sample of candidates can therefore be enriched by means of a selection at this

[3] For cross-matches with cluster catalogues we adopted a larger search radius (5′ instead of 3′) on account of the larger positional uncertainties of clusters compared to those of non-*Planck* point source catalogues used in this paper.

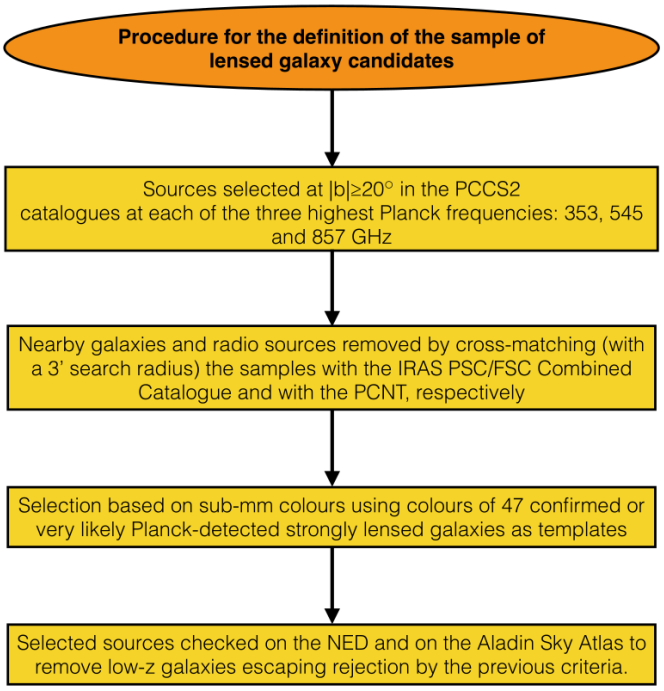

Fig. 5. Flowchart summarizing our procedure to select candidate strongly lensed galaxies.

frequency that favours lower zs. The approach we adopted is analogous to that described above, but we exploited the BeeP photometry, which is available for all sources in the PCCS2 857 GHz list and includes 3000 GHz (100 μm) flux densities extracted from the IRIS map[4] at this frequency. Having photometric data both at higher and at lower frequencies improves the accuracy of the photometry at the selection frequency.

Again, we started requiring $|b| \geq 20°$ and removing objects with IRAS or PCNT counterparts, but we kept PCNT sources whose sub-mm emission is dominated by dust. BeeP photometry is available for 23 confirmed or very likely strongly lensed galaxies. Except for a few outliers with low S/Ns, hence with very uncertain colours, these objects have $S_{857}/S_{545} < 2.75$ (one outlier), $S_{857}/S_{3000} > 2.5$ (two outliers, including the previous one), detection significance SRCSIG ≥ 5 and $S_{857} < 2.65$ Jy. We used these limits to select candidate strongly lensed galaxies, except for conservatively relaxing the one on S_{857} to $S_{857} < 3$ Jy and adding the requirement SNRR > 1 at each frequency, 353, 545 and 857 GHz[5]. These criteria yielded a sample of 133 sources, including 21 confirmed or very likely strongly lensed objects (one confirmed strongly lensed galaxy with $S_{857}/S_{545} < 2.75$ has $S/N_{353} < 1$).

Without the 25 sources that are included in the 545 GHz sample (Table A.1) and the 11 local galaxies we found by searching for objects on the NED, we have a sample of 97 objects. We list them in Table A.2, including 8 that are confirmed or very likely lensed. The last column of Table A.2 shows that we have seven matches with the GCC catalogue, one of which is a confirmed strongly lensed galaxy. We also have two matches with the PHz catalogue, including a confirmed strongly lensed galaxy. There are no matches with *Planck* SZ clusters. There are, however, four associations within 5 arcmin with at least one of the catalogues mentioned in Sect. 2.2. These sources are tagged with a C label in the last column of Table A.2.

Eleven of the 97 objects lie in the SPT area. Four of these have an SPT match, including the strongly lensed galaxy at RA = 17.4822 deg, Dec = −47.0149. The source at RA = 92.9950, Dec = −55.2434 can be identified with the strongly lensed galaxy DES J0611−5514 at $z = 0.7$ (Diehl et al. 2017) at an angular separation of 0.76 arcmin, which is well within the *Planck* positional error. The other 2 objects are unresolved by the SPT, have no nearby galaxy counterpart, and therefore may well be at high-z, that is, are strongly lensed. Of the 7 objects without SPT counterpart, 3 (80.5288, −64.4013; 89.9582, −40.4288; and 332.4487, −58.7876) are located in cirrus regions; the other 4 might be CIB fluctuations or proto-clusters of dusty galaxies. When we restrict ourselves to $S_{857}/S_{545} < 2.3$ (75 sources), we have 8 sources in the SPT area, including the 4 with SPT counterparts. In this case, the selection efficiency for strongly lensed galaxies is between 25% and 50%.

2.4. Selection at 353 GHz

The 353 GHz selection favours higher-z sources. Similarly to what we did at 545 GHz, we started from the PCCS2 353 GHz catalogue and selected objects at $|b| \geq 20°$. We removed nearby galaxies by removing matches with the IRAS PSC/FSC Combined Catalogue (Abrahamyan et al. 2015) and radio sources by removing matches with the PCNT (Planck Collaboration Int. LIV 2018) within a 3 arcmin search radius, except for sources whose sub-mm emission is dominated by dust (6 objects). This yielded a sample of 512 sources, including 19 confirmed or very likely strongly lensed galaxies. As expected, the latter have redder colours than those selected at the two higher frequencies: all of them have $S_{857}/S_{545} < 2$. For consistency with the previous choices, we adopted $S_{857}/S_{545} < 2.3$ to select candidate strongly lensed galaxies.

Removing sources in the 545 and 857 GHz samples (29 and 5 objects, respectively), we are left with 478 sources for which we obtained MTXF photometry. The condition $S_{857}/S_{545} < 2.3$ leaves 228 objects. We further required an S/N at 353 GHz $S/N_{353} > 3$ and dropped the 3 sources that we found by searching the NED to be associated with low-z galaxies. The final sample, containing 104 objects, is presented in Table A.3. Thirteen of the sources in this sample have a *Planck* SZ cluster within 5 arcmin. A cross-match with the catalogues mentioned in Sect. 2.2 yielded 4 additional associations with galaxy clusters. These 17 sources are tagged with a C label in the last column of Table A.3. We also have 6 matches with the PHz catalogue and 7 matches with the GCC catalogue.

Twenty-one of the 104 sources in the final sample lie in the SPT area, and 5 of them have SPT counterparts within 3 arcmin. The matches include 2 high-z sources at RA, Dec in degrees (82.2573, −54.6264) and (87.4900, −53.9362) with $z = 3.3689$ and $z = 3.128$, respectively. They can be safely regarded as previously unrecognized *Planck*-detected strongly lensed galaxies. Two sources (41.3710, −53.0432 and 353.0972, −53.9802) have galaxy clusters in the *Planck* SZ catalogue along their lines of sight. The Everett et al. (2020) catalogue identifies them with cluster members. However, the cluster redshifts ≃0.3 and ≃0.4 are in the zone of avoidance in Fig. 2, that is, they are either too high or too low to belong to the *Planck* sources. The *Planck* sources are instead likely background galaxies lensed by the

[4] The Improved Reprocessing of the IRAS Survey (IRIS) maps are reprocessed IRAS maps generated by Miville-Deschênes & Lagache (2005).

[5] The SNRR at a given frequency is defined by Planck Collaboration Int. LV (2020) as the source average brightness divided the background standard deviation brightness. The source detection significance is measured by SRCSIG.

clusters. The fifth source (338.2416, −61.2784) is unresolved by the SPT and lacks any optical identification, suggesting that it is a high-z dust-enshrouded galaxy.

Two out of the 16 sources in the SPT area lacking an SPT identification (those at 15.7465, −49.2554 and 342.2042, −44.5310) are associated in projection with *Planck* SZ clusters. A search in the NED has revealed that the first source has a $z = 4.16$ galaxy in the background of the "El Gordo" cluster at $z \simeq 0.87$ as a possible counterpart. The region along the line of sight of the second source is very complex. It contains the cluster Abell S1063 at $z = 0.3475$ and other overdensities at $z = 0.742$, $z \simeq 1.2$ and $z \simeq 3.2$. Several strongly lensed galaxies have been discovered in this region, with z of up to ≃3. Our source might be one of them, or it may consist of the summed emission of dusty galaxies in high-z overdensities. The source at (41.3768, −64.3372) can be identified with the PHz source G284−48.60, a candidate high-z proto-cluster of dusty galaxies.

Above $S/N_{353} > 4$, we have 41 sources, 14 of which lie in the SPT area, with the same 5 SPT matches and the same associations with SZ clusters. A selection efficiency between ∼35% and ∼50% for very likely strongly lensed galaxies is thus indicated in this case.

3. Discussion and conclusions

As a result of a systematic search for extreme strongly lensed galaxies in the *Planck* catalogues, we have produced lists of candidates selected at each of the three highest *Planck* frequencies, 353, 545, and 857 GHz. Our approach took advantage of the fact that without the flux boosting by extreme gravitational lensing, the shallow *Planck* surveys at these frequencies detect only nearby ($z \lesssim 0.1$) dusty galaxies. Only at $z \gtrsim 1$ are there enough ultraluminous galaxies and a sufficiently large lensing optical depth to allow galaxies with extreme magnifications (of up to a factor of 50; Cañameras et al. 2015) to be detectable by *Planck*, however, taking advantage also of the strongly negative K-correction. The wide redshift gap between these two populations implies that they have quite different sub-mm colours. High-z galaxies are substantially redder on average, although measurement errors blur the difference.

We started by selecting sources at $|b| \geq 20°$ in the PCCS2 catalogues at each of the three frequencies. Next, we removed nearby galaxies and radio sources identified by cross-matching the samples with the IRAS PSC/FSC Combined Catalogue (Abrahamyan et al. 2015) and with the PCNT (Planck Collaboration Int. LIV 2018), respectively, using a 3 arcmin search radius.

Even with the benefit of extreme gravitational magnifications, the flux densities of strongly lensed galaxies are close to the detection limits. They therefore rarely have PCCS2 measurements at all frequencies ≥353 GHz, which is necessary to compute the colours. To solve this problem, we exploited the new BeeP multifrequency photometry (Planck Collaboration Int. LV 2020), which is also constrained by the IRAS 3000 GHz photometry, for the sample selected at 857 GHz. At the two lower frequencies at which the BeeP photometry is available only for a subset of sources, we obtained new MTXF multifrequency photometry. The sub-mm colours of 47 confirmed or very likely *Planck*-detected strongly lensed galaxies were used as a benchmark to select the colour range of the lensed candidates. All sources in the colour–selected samples were confirmed on the NED to remove those that are associated with low-z galaxies that escaped rejection by the adopted criteria.

Our main sample, selected at 545 GHz, comprises 177 lensed candidates (Table A.1). The sample selected at 857 GHz contains 97 sources after we excluded those in the 545 GHz sample (Table A.2). The sample at 353 GHz contains 104 sources (Table A.3), excluding those in the other two samples.

A test of the efficiency of our approach in selecting strongly lensed galaxies was made considering that within the area covered by the SPT survey (≃2500 deg^2; Everett et al. 2020), 14 out of 19 sources selected with our method are either classified as strongly lensed by independent data (3) or can be safely regarded as previously unrecognized *Planck*-detected strongly lensed galaxies. This area includes 47 candidates, therefore the selection efficiency is in the range 30−40%. We discussed stricter selection criteria that increase the efficiency to ≃50% at the cost of a somewhat lower completeness: the stricter criteria miss ≃10% of the confirmed plus very likely strongly lensed galaxies recovered by the baseline criteria.

Another test can be made with reference to the H-ATLAS survey that covers ≃600 deg^2. Thirteen of the objects selected with our method lie within the H-ATLAS fields. Three of them, those at (RA, Dec: 176.6239, −0.22157; 201.6254, 33.7353; and 206.1251, 30.5058), are confirmed strongly lensed galaxies (Negrello et al. 2017), corresponding to an efficiency of ≃23%, although with poor statistics (1σ range 11−46%).

The other ten sources have an H-ATLAS match within 3 arcmin. The *Herschel*/SPIRE flux densities of the matched sources are too faint to be identified with the *Planck* sources (all have F500BEST < 80 mJy)[6], however. Their colours are red, and they lack possible identifications with low-z galaxies. This suggests that *Planck* detections are high-z overdensities, to which H-ATLAS sources belong.

Our analysis shows that probably more than 50% of sources in our samples are not strongly lensed galaxies, but a mixture of other objects with cold SEDs, such as high-z proto-clusters of dusty galaxies, Galactic cold clumps, CIB fluctuations, and Galactic cirrus. Unfortunately, we cannot exploit specific searches for these objects to clean the samples. However, the discovery of new proto-clusters and GCCs by following-up our candidates would also be a very interesting scientific result.

Planck Collaboration Int. XXXIX (2016) published a catalogue of 2151 sources with red sub-mm colours, indicative of $z > 2$. These high-z source candidates were extracted from *Planck* high-frequency maps over the 25.8% of the sky with minimum thermal emission from Galactic dust. The source detection was made using a specific component-separation procedure that allowed a much better sensitivity to this class of sources than the PCCS2. Planck Collaboration Int. XXVII (2015), based on the *Herschel* follow-up of 228 *Planck* high-z source candidates, stated that more than 93% of them are galaxy overdensities, that is, candidate proto-clusters of dusty galaxies, and 3% are strongly lensed individual galaxies. At first sight, this suggests that we might exploit the PHz to remove candidate proto-clusters from our samples, or at least to estimate their fraction.

However, as already pointed out by Planck Collaboration Int. XXXIX (2016), the overlap between the PHz and the PCCS2 is extremely small. By cross-matching the PHz with the PCCS2 catalogues at 353, 545, and 857 GHz, we found only 29 distinct associations. Of these, 21 meet our selection criteria, including 8 confirmed (7 sources) or very likely (1 source) strongly lensed galaxies. The fraction of strongly lensed galaxies of the

[6] In the H-ATLAS Catalog, F500BEST is the 500 μm best flux that is defined as the largest of the aperture or point source flux, taking into account the noise.

PHz sources that are included in the PCCS2 is thus far larger than in the general PHz catalogue. Taking the strong incompleteness of the sample of confirmed strongly lensed galaxies into account, they may well be the majority in the PCCS2 sub-sample of the PHz, and even more after our selection. Nevertheless, our cross-matches with the SPT and H-ATLAS catalogues have highlighted that some of our high-z candidates may be resolved by the SPT or by *Herschel* and may therefore be proto-clusters that are not included in the PHz catalogue.

Another population that can meet our selection criteria because of their red sub-mm colours, similar to those of high-z sources, are Galactic cold clumps (Planck Collaboration XXVIII 2016). Most of them are found close to the Galactic plane, but some were detected at high Galactic latitude as well. We found 99 matches within 3 arcmin between the GCC catalogue and the PCCS2. Thirty-four of them, including 8 confirmed strongly lensed galaxies, meet our selection criteria. The substantial fraction of strongly lensed galaxies obviously implies that the presence in the GCC catalogue cannot be a valid criterion for excluding sources from our lists. On the other hand, these objects are of great interest per se because they provide key information on the early phases of star formation (Planck Collaboration XXVIII 2016).

Most published model predictions at sub-mm wavelengths (Perrotta et al. 2002, 2003; Negrello et al. 2007, 2017; Béthermin et al. 2011; Cai et al. 2013) refer to galaxy-galaxy lensing. In this case, a maximum magnification $\mu_{\rm max} \simeq 15$ is indicated by the data (see Fig. 7 of Negrello et al. 2017). The extreme magnifications of *Planck* strongly lensed galaxies can be understood in terms of lensing by galaxy groups or clusters (Frye et al. 2019), however.

Figure 6 shows our estimate of the integral number counts of strongly lensed galaxies detected by *Planck*, compared to observed and predicted counts of galaxy-galaxy lensed galaxies at 500 μm (600 GHz). This estimate was obtained as follows. The 90% completeness flux density limit at our reference frequency of 545 GHz is $S_{545,\rm lim} \simeq 500$ mJy (Planck Collaboration XXVI 2016; Maddox et al. 2018). We can identify *Planck*-detected strongly lensed galaxies with good completeness and reliability only in areas that rare covered by deeper, higher angular resolution surveys, that is, over the 3100 deg^2 surveyed by the SPT plus H-ATLAS. We have 11 such sources in this area, 7 of which have a flux density above $S_{545,\rm lim}$. For a typical redshift $z \simeq 2$, the proto-spheroidal SED by Cai et al. (2013) yields $S_{500\,\mu\rm m}/S_{545\,\rm GHz} = 1.2$. After correcting for the 10% incompleteness, we find $N(>500\,\rm mJy) = 2.5(+1.3, -0.8) \times 10^{-3}$ deg^{-2} at 500 μm, with Poisson errors computed following Gehrels (1986).

The figure shows that the counts of *Planck* strongly lensed galaxies indeed exceed the extrapolation of observed counts and model predictions, both referring to galaxy-galaxy lensing. The important role of galaxy-cluster lensing is supported by the results of our cross-match with cluster catalogues. We have found a total of 20 associations of our lensed candidate samples with the *Planck* SZ catalogue (Planck Collaboration XXVII 2016). This catalogue is not deep enough for a thorough search for associations, but it the best available option at the moment while we wait for the eROSITA cluster survey. Deeper catalogues cover a small fraction of the sky. The *Planck* SZ catalogue contains 1653 clusters spread over ≃34 500 deg^2. Their mean surface density is thus of ≃0.048 clusters deg^{-2}. The number of chance associations within the total searched area $\simeq\pi(5/60)^2 \times N_{\rm cand} \simeq 8.2$ deg^2, $N_{\rm cand} = 377$ being the sum of candidates in our 3 samples, is 0.39. The Poisson probability of having by chance 20 associations when the expected number is 0.39 is vanishingly small, confirming that our candidates have a strong excess of foreground clusters.

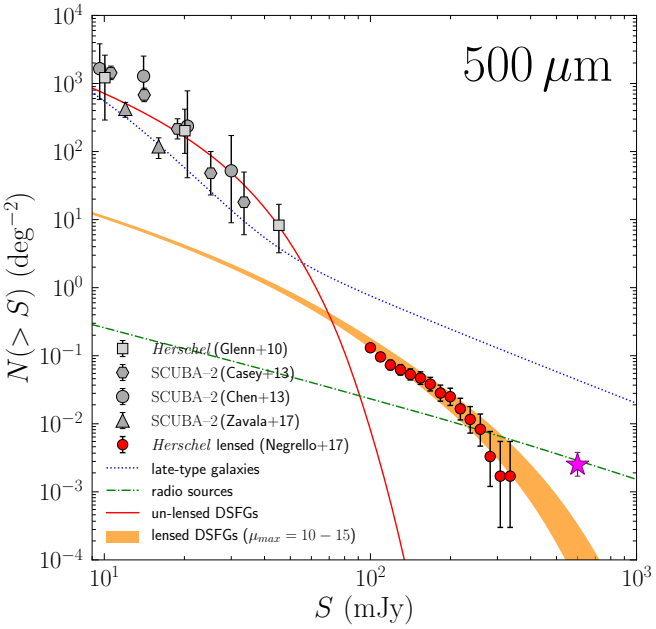

Fig. 6. Contributions of different source populations, specified in the legend, to the integral number counts at 500 μm (600 GHz), compared with observational data. The counts of late-type, normal, and starburst galaxies and of unlensed dusty star-forming galaxies (DSFGs), interpreted as proto-spheroidal galaxies in the process of forming the bulk of their stars, are from the Cai et al. (2013) model. The orange band shows the counts of strongly lensed (magnification $\mu > 2$) DSFGs recomputed by Negrello et al. (2017) for magnification cut-offs, $\mu_{\rm max}$, in the range 10−15. The calculations were made exploiting the Cai et al. (2013) model coupled with the Lapi et al. (2012) formalism to include galaxy-galaxy lensing. The counts of radio sources (dot-dashed green line) are from the Tucci et al. (2011) model. The data points are from Glenn et al. (2010), Chen et al. (2013), Casey et al. (2013), and Zavala et al. (2017). The purple star in the bottom right corner shows our estimate of the counts of *Planck*-detected strongly lensed galaxies. As expected, these counts exceed predictions for galaxy-galaxy lensing, consistent with being mostly contributed by galaxy-cluster lensing. Adapted from Fig. 8 of Negrello et al. (2017).

Unfortunately, calculations including magnifications by galaxy clusters (Lima et al. 2010; Er et al. 2013) use outdated models and do not extend their predictions to the flux densities of interest here. A proper comparison of our count estimate with model predictions is therefore precluded at this stage.

To summarize, some useful indications are provided for the expected number of *Planck*-detected strongly lensed galaxies by the cross-matches with the SPT and H-ATLAS surveys. The two surveys contain a total of 17−22 confirmed or very likely strongly lensed galaxies detected by *Planck* over an area of 3100 deg^2. This corresponds to 149−192 such objects over the full area at $|b| > 20°$ (≃2.71×10^4 deg^2).

We conclude that *Planck*-detected strongly lensed galaxies constitute a rich enough sample to provide a uniquely detailed view of the internal structure and kinematics of galaxies across the peak of the cosmic star formation through high-resolution spectrophotometric follow up. Moreover, this sample can be exploited to study the spatial distribution of dark and luminous mass in galaxies or galaxy clusters acting as lenses over

a broader redshift range than is possible with optically selected strongly lensed galaxies.

Follow-up work on candidates has started. SCUBA-2 photometric observations at 850 μm (353 GHz) of a preliminary selection (proposal ID: M19BP010, P.I.: M. Negrello) have already been mentioned; four of the detected sources were observed spectroscopically with the Northern Extended Millimeter Array (NOEMA; Proposal ID: S20BQ, P.I.: M. Negrello). Other samples were observed with the Australia Telescope Compact Array (ATCA) at 5.5 and 94 GHz (project ID C3301, P.I.: M. Bonato, 95 h of observing time) and with the IRAM second-generation Neel-IRAM-KID-Array (NIKA 2) at 1 and 2 mm (project ID 212-19, P.I.: M. Bonato, 13.5 h of observing time). The analysis of these data is in progress.

Acknowledgements. We are grateful to the anonymous referee for useful comments. DH thanks the Spanish Ministerio de Ciencia, Innovación y Universidades for partial financial support under project PGC2018-101814-B-I00. MB acknowledges support from INAF under PRIN SKA/CTA FORECaST, from the Ministero degli Affari Esteri e della Cooperazione Internazionale – Direzione Generale per la Promozione del Sistema Paese Progetto di Grande Rilevanza ZA18GR02 and from the South African Department of Science and Technology's National Research Foundation (DST-NRF Grant Number 113121). This research has made use of the *Planck* Legacy Archive (`https://www.cosmos.esa.int/web/planck/pla`), of the TOPCAT software (Taylor 2005), of the Aladin Sky Atlas developed at CDS, Strasbourg Observatory, France, and of the NASA/IPAC Extragalactic Database (NED). *Planck* is an ESA science mission with instruments and contributions directly funded by ESA Member States, NASA, and Canada. The NED is operated by the Jet Propulsion Laboratory, California Institute of Technology, under contract with the National Aeronautics and Space Administration.

References

Abrahamyan, H. V., Mickaelian, A. M., & Knyazyan, A. V. 2015, Astron. Comput., 10, 99
Bakx, T. J. L. C., Eales, S., & Amvrosiadis, A. 2020, MNRAS, 493, 4276
Béthermin, M., Dole, H., Lagache, G., Le Borgne, D., & Penin, A. 2011, A&A, 529, A4
Bleem, L. E., Stalder, B., de Haan, T., et al. 2015, ApJS, 216, 27
Boch, T., & Fernique, P. 2014, in Astronomical Data Analysis Software and Systems XXIII, eds. N. Manset, & P. Forshay, ASP Conf. Ser., 485, 277
Bonnarel, F., Fernique, P., Bienaymé, O., et al. 2000, A&AS, 143, 33
Bourne, N., Dunne, L., Maddox, S. J., et al. 2016, MNRAS, 462, 1714
Cañameras, R., Nesvadba, N. P. H., Guery, D., et al. 2015, A&A, 581, A105
Cañameras, R., Nesvadba, N. P. H., Kneissl, R., et al. 2017a, A&A, 600, L3
Cañameras, R., Nesvadba, N., Kneissl, R., et al. 2017b, A&A, 604, A117
Cañameras, R., Nesvadba, N. P. H., Limousin, M., et al. 2018a, A&A, 620, A60
Cañameras, R., Yang, C., Nesvadba, N. P. H., et al. 2018b, A&A, 620, A61
Cañameras, R., Nesvadba, N. P. H., Kneissl, R., et al. 2021, A&A, 645, A45
Cai, Z.-Y., Lapi, A., Xia, J.-Q., et al. 2013, ApJ, 768, 21
Cao, X., Li, R., Shu, Y., et al. 2020, MNRAS, 499, 3610
Casey, C. M., Chen, C.-C., Cowie, L. L., et al. 2013, MNRAS, 436, 1919
Chen, C.-C., Cowie, L. L., Barger, A. J., et al. 2013, ApJ, 776, 131
Dannerbauer, H., Harrington, K., Díaz-Sánchez, A., et al. 2019, AJ, 158, 34
Delabrouille, J., Betoule, M., Melin, J. B., et al. 2013, A&A, 553, A96
Díaz-Sánchez, A., Iglesias-Groth, S., Rebolo, R., & Dannerbauer, H. 2017, ApJ, 843, L22
Diehl, H. T., Buckley-Geer, E. J., Lindgren, K. A., et al. 2017, ApJS, 232, 15
Eales, S., Dunne, L., Clements, D., et al. 2010, PASP, 122, 499
Enia, A., Negrello, M., Gurwell, M., et al. 2018, MNRAS, 475, 3467
Er, X., Li, G., Mao, S., & Cao, L. 2013, MNRAS, 430, 1423
Everett, W. B., Zhang, L., Crawford, T. M., et al. 2020, ApJ, 900, 55
Finoguenov, A., Rykoff, E., Clerc, N., et al. 2020, A&A, 638, A114
Frye, B. L., Pascale, M., Qin, Y., et al. 2019, ApJ, 871, 51
Fu, H., Jullo, E., Cooray, A., et al. 2012, ApJ, 753, 134
Fujimoto, S., Ouchi, M., Kohno, K., et al. 2018, ApJ, 861, 7
Fujimoto, S., Silverman, J. D., Bethermin, M., et al. 2020, ApJ, 900, 1
Gehrels, N. 1986, ApJ, 303, 336
Glenn, J., Conley, A., Béthermin, M., et al. 2010, MNRAS, 409, 109
Gonzalez, A. H., Gettings, D. P., Brodwin, M., et al. 2019, ApJS, 240, 33
González-Nuevo, J., Lapi, A., Fleuren, S., et al. 2012, ApJ, 749, 65
González-Nuevo, J., Suárez Gómez, S. L., Bonavera, L., et al. 2019, A&A, 627, A31
Gruppioni, C., Pozzi, F., Rodighiero, G., et al. 2013, MNRAS, 432, 23
Harrington, K. C., Yun, M. S., Cybulski, R., et al. 2016, MNRAS, 458, 4383
Harrington, K. C., Yun, M. S., Magnelli, B., et al. 2018, MNRAS, 474, 3866
Harrington, K. C., Vishwas, A., Weiß, A., et al. 2019, MNRAS, 488, 1489
Harrington, K. C., Weiss, A., Yun, M. S., et al. 2021, ApJ, 908, 95
Herranz, D., González-Nuevo, J., Clements, D. L., et al. 2013, A&A, 549, A31
Hezaveh, Y. D., & Holder, G. P. 2011, ApJ, 734, 52
Hilbert, S., White, S. D. M., Hartlap, J., & Schneider, P. 2008, MNRAS, 386, 1845
Hilton, M., Sifón, C., Naess, S., et al. 2021, ApJS, 253, 3
Hodge, J. A., Swinbank, A. M., Simpson, J. M., et al. 2016, ApJ, 833, 103
Ikarashi, S., Caputi, K. I., Ohta, K., et al. 2017, ApJ, 849, L36
Jarrett, T. H., Cluver, M. E., Magoulas, C., et al. 2017, ApJ, 836, 182
Jones, G. C., Maiolino, R., Caselli, P., & Carniani, S. 2019, A&A, 632, L7
King, A., & Pounds, K. 2015, ARA&A, 53, 115
Lagache, G., Puget, J.-L., & Dole, H. 2005, ARA&A, 43, 727
Lapi, A., Negrello, M., González-Nuevo, J., et al. 2012, ApJ, 755, 46
Lima, M., Jain, B., Devlin, M., & Aguirre, J. 2010, ApJ, 717, L31
Maddox, S. J., Valiante, E., Cigan, P., et al. 2018, ApJS, 236, 30
Merloni, A., Predehl, P., Becker, W., et al. 2012, ArXiv e-prints [arXiv:1209.3114]
Miville-Deschênes, M.-A., & Lagache, G. 2005, ApJS, 157, 302
Mocanu, L. M., Crawford, T. M., Vieira, J. D., et al. 2013, ApJ, 779, 61
Nayyeri, H., Keele, M., Cooray, A., et al. 2016, ApJ, 823, 17
Negrello, M., Perrotta, F., González-Nuevo, J., et al. 2007, MNRAS, 377, 1557
Negrello, M., Hopwood, R., De Zotti, G., et al. 2010, Science, 330, 800
Negrello, M., Clemens, M., Gonzalez-Nuevo, J., et al. 2013, MNRAS, 429, 1309
Negrello, M., Amber, S., Amvrosiadis, A., et al. 2017, MNRAS, 465, 3558
Nesvadba, N., Kneissl, R., Cañameras, R., et al. 2016, A&A, 593, L2
Nesvadba, N. P. H., Cañameras, R., Kneissl, R., et al. 2019, A&A, 624, A23
Oliver, S. J., Bock, J., Altieri, B., et al. 2012, MNRAS, 424, 1614
Perrotta, F., Baccigalupi, C., Bartelmann, M., De Zotti, G., & Granato, G. L. 2002, MNRAS, 329, 445
Perrotta, F., Magliocchetti, M., Baccigalupi, C., et al. 2003, MNRAS, 338, 623
Piffaretti, R., Arnaud, M., Pratt, G. W., Pointecouteau, E., & Melin, J. B. 2011, A&A, 534, A109
Planck Collaboration VII. 2011, A&A, 536, A7
Planck Collaboration XV. 2014, A&A, 571, A15
Planck Collaboration I. 2016, A&A, 594, A1
Planck Collaboration XXVI. 2016, A&A, 594, A26
Planck Collaboration XXVII. 2016, A&A, 594, A27
Planck Collaboration XXVIII. 2016, A&A, 594, A28
Planck Collaboration I. 2020, A&A, 641, A1
Planck Collaboration Int. VII. 2013, A&A, 550, A133
Planck Collaboration Int. XXVII. 2015, A&A, 582, A30
Planck Collaboration Int. XXXIX. 2016, A&A, 596, A100
Planck Collaboration Int. LIV. 2018, A&A, 619, A94
Planck Collaboration Int. LV. 2020, A&A, 644, A99
Reuter, C., Vieira, J. D., Spilker, J. S., et al. 2020, ApJ, 902, 78
Robertson, A., Smith, G. P., Massey, R., et al. 2020, MNRAS, 495, 3727
Rowan-Robinson, M., Wang, L., Farrah, D., et al. 2018, A&A, 619, A169
Shibuya, T., Ouchi, M., & Harikane, Y. 2015, ApJS, 219, 15
Shibuya, T., Ouchi, M., Harikane, Y., & Nakajima, K. 2019, ApJ, 871, 164
Shu, Y., Bolton, A. S., Kochanek, C. S., et al. 2016, ApJ, 824, 86
Silk, J., & Mamon, G. A. 2012, Res. Astron. Astrophys., 12, 917
Somerville, R. S., & Davé, R. 2015, ARA&A, 53, 51
Spilker, J. S., Marrone, D. P., Aravena, M., et al. 2016, ApJ, 826, 112
Spilker, J. S., Aravena, M., Béthermin, M., et al. 2018, Science, 361, 1016
Spilker, J. S., Phadke, K. A., Aravena, M., et al. 2020, ApJ, 905, 85
Sun, F., Egami, E., Rawle, T. D., et al. 2021, ApJ, 908, 192
Swinbank, A. M., Smail, I., Longmore, S., et al. 2010, Nature, 464, 733
Talbot, M. S., Brownstein, J. R., Dawson, K. S., Kneib, J.-P., & Bautista, J. 2021, MNRAS, 502, 4617
Taylor, M. B. 2005, in Astronomical Data Analysis Software and Systems XIV, eds. P. Shopbell, M. Britton, & R. Ebert, ASP Conf. Ser., 347, 29
Tucci, M., Toffolatti, L., de Zotti, G., & Martínez-González, E. 2011, A&A, 533, A57
Veilleux, S., Maiolino, R., Bolatto, A. D., & Aalto, S. 2020, A&ARv, 28, 2
Vieira, J. D., Crawford, T. M., Switzer, E. R., et al. 2010, ApJ, 719, 763
Viero, M. P., Asboth, V., Roseboom, I. G., et al. 2014, ApJS, 210, 22
Wardlow, J. L., Cooray, A., De Bernardis, F., et al. 2013, ApJ, 762, 59
Weiß, A., De Breuck, C., Marrone, D. P., et al. 2013, ApJ, 767, 88
Zavala, J. A., Aretxaga, I., Geach, J. E., et al. 2017, MNRAS, 464, 3369

Appendix A: Candidate strongly lensed galaxies selected at 545, 857, and 353 GHz

Table A.1. MTXF photometry of candidate strongly lensed galaxies selected at 545 GHz.

Planck name	RA	DEC	S_{217}	S_{353}	S_{545}	S_{857}	S_{857}/S_{545}	S_{545}/S_{353}	Note
PG107.82-45.46	1.8930	16.1184	135 ± 33	567 ± 83	922 ± 131	1213 ± 334	1.32	1.62	G,C
PG318.60-68.18	4.2517	-47.8788	40 ± 26	184 ± 65	414 ± 94	602 ± 151	1.45	2.26	
PG116.05-45.04	7.7692	17.5577	119 ± 50	393 ± 144	1678 ± 417	4470 ± 1327	2.66	4.27	
PG120.01-43.19	10.6032	19.6206	60 ± 36	307 ± 81	610 ± 136	638 ± 339	1.05	1.98	
PG124.53-28.73	14.5626	34.1135	76 ± 37	128 ± 96	623 ± 156	1514 ± 432	2.43	4.85	
PG128.89-71.39	14.7807	-8.6103	67 ± 35	338 ± 79	812 ± 142	2209 ± 385	2.72	2.40	
PG130.16-64.05	16.0164	-1.3606	52 ± 32	179 ± 80	569 ± 122	1269 ± 307	2.23	3.17	
PG215.65-87.14	16.0636	-27.2274	49 ± 29	113 ± 69	553 ± 113	615 ± 254	1.11	4.91	C
PG130.55-46.12	18.3579	16.4231	63 ± 45	167 ± 145	1093 ± 329	2618 ± 911	2.40	6.52	
PG131.05-48.15	18.4473	14.3667	88 ± 38	283 ± 94	913 ± 144	2505 ± 323	2.74	3.22	
PG190.40-83.77	19.1952	-24.6171	58 ± 27	264 ± 67	650 ± 111	1351 ± 260	2.08	2.46	L
PG138.59-65.63	19.2684	-3.5471	76 ± 35	231 ± 112	983 ± 240	2592 ± 776	2.64	4.25	
PG298.30-51.33	19.8435	-65.5378	40 ± 25	204 ± 61	412 ± 106	732 ± 190	1.78	2.01	
PG271.10-79.07	19.9754	-36.2299	42 ± 28	185 ± 75	365 ± 100	627 ± 178	1.72	1.98	
PG139.15-61.54	20.5090	0.3582	96 ± 37	290 ± 84	550 ± 101	576 ± 175	1.05	1.90	C
PG133.90-45.23	20.9152	16.9511	127 ± 64	475 ± 199	1748 ± 605	4739 ± 1710	2.71	3.68	
PG129.75-21.87	21.2065	40.5538	80 ± 39	146 ± 93	615 ± 154	1134 ± 309	1.84	4.22	
PG134.09-44.10	21.2687	18.0403	80 ± 47	375 ± 129	1408 ± 310	3768 ± 940	2.68	3.76	
PG287.12-68.67	21.2802	-47.3991	83 ± 30	271 ± 53	618 ± 102	1078 ± 162	1.74	2.28	L,G,S
PG134.33-43.70	21.5228	18.3991	169 ± 39	359 ± 111	1423 ± 251	3734 ± 682	2.62	3.97	G
PG143.33-54.61	24.5773	6.3845	92 ± 41	259 ± 104	636 ± 169	1591 ± 399	2.50	2.46	
PG137.57-27.57	28.4543	33.5216	57 ± 35	211 ± 75	568 ± 101	794 ± 199	1.40	2.70	
PG156.56-55.28	31.2673	2.7090	46 ± 33	397 ± 91	648 ± 126	1199 ± 207	1.85	1.63	
PG160.59-56.77	32.4206	0.2624	139 ± 35	459 ± 91	885 ± 133	1384 ± 240	1.56	1.93	L,H
PG246.64-70.52	33.0350	-36.4832	59 ± 28	106 ± 65	565 ± 105	1192 ± 179	2.11	5.36	
PG267.97-65.11	33.2111	-46.1033	64 ± 25	172 ± 74	402 ± 103	780 ± 163	1.94	2.34	
PG189.71-67.30	34.5732	-16.5767	120 ± 34	124 ± 84	419 ± 139	872 ± 318	2.08	3.39	
PG249.97-68.08	35.2534	-38.5477	92 ± 27	395 ± 70	704 ± 104	1291 ± 180	1.83	1.78	C
PG254.36-56.45	48.6259	-44.8686	89 ± 31	226 ± 64	638 ± 111	786 ± 193	1.23	2.83	H,S,L
PG273.03-48.77	51.6471	-58.3662	37 ± 28	170 ± 63	634 ± 123	1697 ± 311	2.68	3.74	
PG252.49-48.14	60.4995	-45.8825	47 ± 27	178 ± 55	580 ± 86	1048 ± 153	1.81	3.26	S
PG216.25-45.47	61.5139	-21.1767	70 ± 34	167 ± 72	568 ± 119	1027 ± 235	1.81	3.40	
PG224.54-44.72	63.9801	-26.6254	70 ± 37	201 ± 82	817 ± 140	2000 ± 303	2.45	4.07	G
PG224.66-40.72	68.3356	-25.7670	67 ± 33	125 ± 65	422 ± 102	751 ± 188	1.78	3.37	
PG269.16-40.52	68.3701	-59.1677	57 ± 20	130 ± 47	431 ± 95	895 ± 222	2.07	3.31	S
PG263.13-36.40	77.3063	-55.1791	53 ± 18	223 ± 42	535 ± 100	744 ± 187	1.39	2.40	G,H
PG266.89-34.31	80.7708	-58.3758	21 ± 16	138 ± 41	346 ± 90	599 ± 166	1.73	2.50	S
PG270.96-33.08	82.8274	-61.8279	57 ± 21	145 ± 56	370 ± 179	980 ± 514	2.65	2.54	
PG257.55-31.95	84.5918	-50.5116	66 ± 24	196 ± 53	585 ± 105	955 ± 196	1.63	2.99	S
PG246.14-28.90	86.7513	-40.3237	72 ± 28	283 ± 78	826 ± 162	1873 ± 367	2.27	2.92	G
PG254.73-29.78	87.4533	-47.8454	104 ± 26	340 ± 73	849 ± 177	1935 ± 404	2.28	2.50	S
PG243.63-27.80	87.4816	-37.9216	59 ± 28	123 ± 69	465 ± 140	1188 ± 351	2.56	3.78	
PG245.77-25.95	90.3798	-39.3147	84 ± 32	329 ± 55	773 ± 119	1881 ± 281	2.43	2.35	
PG253.78-24.65	94.5621	-46.0018	80 ± 27	157 ± 64	646 ± 127	1505 ± 311	2.33	4.11	S
PG183.69+23.25	113.2382	35.4110	71 ± 34	271 ± 84	689 ± 130	1538 ± 263	2.23	2.54	
PG169.24+27.10	113.8596	49.0247	49 ± 35	84 ± 83	688 ± 110	1889 ± 258	2.74	8.15	
PG170.60+26.93	113.9615	47.8044	42 ± 35	184 ± 99	543 ± 240	1363 ± 681	2.51	2.95	
PG162.74+28.47	114.5428	54.9187	65 ± 34	298 ± 86	636 ± 130	1506 ± 249	2.37	2.13	
PG173.22+27.77	115.8472	45.6926	177 ± 36	599 ± 92	2248 ± 171	6142 ± 440	2.73	3.75	G
PG157.43+30.34	117.2154	59.6986	48 ± 36	465 ± 70	819 ± 109	1141 ± 250	1.39	1.76	L,G,C

Table A.1. continued.

Planck name	RA	DEC	S_{217}	S_{353}	S_{545}	S_{857}	S_{857}/S_{545}	S_{545}/S_{353}	Note
PGG172.28+30.23	119.1419	46.9228	69 ± 35	202 ± 86	718 ± 169	1887 ± 418	2.63	3.55	
PGG200.95+24.00	120.0011	20.7465	39 ± 29	244 ± 86	841 ± 165	2001 ± 392	2.38	3.45	
PGG204.80+24.05	121.4469	17.5030	54 ± 36	337 ± 103	1118 ± 209	2535 ± 519	2.27	3.32	
PGG205.99+24.29	122.1079	16.5904	61 ± 36	199 ± 93	513 ± 176	894 ± 424	1.74	2.58	
PGG204.03+25.05	122.1371	18.5330	97 ± 36	280 ± 82	1098 ± 155	2442 ± 396	2.22	3.93	
PGG203.76+25.22	122.2073	18.8163	84 ± 37	189 ± 86	733 ± 162	1628 ± 409	2.22	3.88	
PGG169.87+32.96	122.8599	49.2810	79 ± 33	177 ± 85	335 ± 96	355 ± 206	1.06	1.89	
PGG206.60+24.99	123.0048	16.3534	132 ± 36	494 ± 107	1547 ± 250	3928 ± 676	2.54	3.13	
PGG175.85+34.02	125.0820	44.4130	105 ± 32	471 ± 112	1139 ± 262	2996 ± 681	2.63	2.42	
PGG198.65+30.95	126.3556	25.0100	69 ± 36	407 ± 112	970 ± 223	2599 ± 555	2.68	2.38	G
PGG197.54+31.39	126.5022	26.0435	100 ± 47	436 ± 193	1148 ± 540	2772 ± 1436	2.41	2.63	
PGG197.08+31.69	126.6979	26.5138	50 ± 44	475 ± 186	1325 ± 504	3323 ± 1251	2.51	2.79	
PGG198.25+31.82	127.1625	25.5988	89 ± 49	161 ± 141	768 ± 373	2083 ± 1029	2.71	4.76	
PGG197.00+32.17	127.1862	26.7119	121 ± 37	258 ± 117	1154 ± 313	2863 ± 790	2.48	4.47	
PGG197.74+32.09	127.3076	26.0884	80 ± 48	433 ± 168	1136 ± 489	2971 ± 1296	2.62	2.62	
PGG195.80+33.01	127.7840	27.9215	67 ± 32	320 ± 79	944 ± 157	2461 ± 377	2.61	2.95	
PGG197.93+32.51	127.8007	26.0606	96 ± 45	190 ± 116	988 ± 237	2570 ± 670	2.60	5.20	
PGG197.69+32.58	127.8205	26.2703	82 ± 37	171 ± 93	773 ± 172	1995 ± 401	2.58	4.51	
PGG216.43+28.25	129.7525	9.6715	54 ± 33	229 ± 78	886 ± 118	2123 ± 258	2.40	3.87	
PGG226.21+24.95	130.9234	0.4012	87 ± 36	315 ± 84	626 ± 126	1082 ± 243	1.73	1.99	
PGG227.25+24.70	131.1897	-0.5411	67 ± 32	152 ± 88	633 ± 132	1709 ± 271	2.70	4.17	
PGG155.14+37.24	131.4813	61.0948	41 ± 34	56 ± 80	387 ± 126	981 ± 316	2.53	6.94	
PGG211.62+32.22	131.7091	15.0964	101 ± 36	494 ± 80	1387 ± 100	2347 ± 190	1.69	2.81	L,G,H,C
PGG229.62+28.51	135.5394	-0.4026	73 ± 31	190 ± 81	504 ± 110	986 ± 221	1.96	2.65	
PGG240.21+22.31	135.7292	-11.7916	61 ± 35	209 ± 84	479 ± 108	1216 ± 265	2.54	2.29	
PGG141.17+36.19	137.7384	72.0643	110 ± 34	274 ± 84	1045 ± 199	2843 ± 582	2.72	3.82	
PGG235.21+29.01	138.6241	-4.2427	57 ± 32	189 ± 68	443 ± 102	920 ± 177	2.08	2.34	
PGG244.13+26.10	141.0334	-12.3201	90 ± 30	259 ± 85	470 ± 107	802 ± 239	1.71	1.81	C
HG200.61+46.09	143.0986	27.4164	143 ± 36	328 ± 78	531 ± 97	672 ± 188	1.27	1.62	L,H,G
PGG219.59+46.00	147.3224	14.8556	80 ± 32	296 ± 81	744 ± 107	1354 ± 222	1.82	2.52	H
PGG170.37+50.67	149.4196	47.2408	115 ± 38	242 ± 59	490 ± 84	772 ± 157	1.58	2.03	C
PGG260.85+25.21	151.3664	-23.7921	89 ± 30	25 ± 76	657 ± 127	1363 ± 319	2.07	26.15	
PGG261.94+25.88	152.6572	-23.9099	47 ± 30	269 ± 81	1026 ± 153	2406 ± 435	2.35	3.81	
PGG259.53+29.69	153.5413	-19.6195	35 ± 31	173 ± 84	723 ± 118	1235 ± 228	1.71	4.19	
PGG219.12+53.25	154.1703	17.9334	56 ± 34	124 ± 83	804 ± 121	2115 ± 268	2.63	6.46	
PGG176.13+55.77	155.1324	42.5998	65 ± 36	230 ± 61	511 ± 86	960 ± 175	1.88	2.22	
PGG153.57+49.93	155.4315	57.3361	46 ± 31	198 ± 72	693 ± 119	1904 ± 297	2.75	3.50	
PGG262.97+31.92	157.4739	-19.7460	70 ± 28	282 ± 64	584 ± 111	619 ± 180	1.06	2.07	
PGG153.55+52.84	159.7831	55.6868	38 ± 35	54 ± 62	342 ± 90	510 ± 149	1.49	6.34	
PGG271.86+25.51	160.5262	-29.4442	63 ± 34	307 ± 81	824 ± 132	1755 ± 283	2.13	2.69	
PGG229.85+57.45	160.7936	14.1816	86 ± 34	220 ± 71	619 ± 110	1248 ± 193	2.02	2.81	
PGG220.55+60.08	161.1953	19.6531	120 ± 39	472 ± 97	1142 ± 219	2578 ± 538	2.26	2.42	G
PGG272.64+25.87	161.4368	-29.5054	170 ± 34	290 ± 78	626 ± 142	1580 ± 324	2.52	2.16	
PGG220.46+60.39	161.4863	19.8032	119 ± 35	316 ± 116	808 ± 230	1591 ± 563	1.97	2.56	
PGG247.35+51.65	162.0435	2.6087	75 ± 32	86 ± 69	279 ± 88	454 ± 153	1.63	3.23	
PGG274.26+25.75	162.8163	-30.3445	50 ± 29	295 ± 66	634 ± 108	1295 ± 199	2.04	2.15	
PGG145.25+50.84	163.3439	60.8635	139 ± 31	505 ± 64	862 ± 114	1032 ± 215	1.20	1.71	L,C
PGG244.76+54.94	163.4709	5.9392	62 ± 29	370 ± 64	1027 ± 108	1852 ± 197	1.80	2.77	L
PGG246.74+57.17	165.8991	6.5869	54 ± 31	183 ± 77	720 ± 146	1507 ± 299	2.09	3.93	
PGG238.49+64.28	169.0560	14.1354	93 ± 26	69 ± 62	388 ± 102	691 ± 183	1.78	5.62	
PGG253.27+59.69	170.1151	5.9120	45 ± 33	363 ± 101	1180 ± 220	2823 ± 468	2.39	3.25	
PGG199.44+69.85	170.1180	29.9714	44 ± 30	75 ± 76	508 ± 94	829 ± 175	1.63	6.76	

Table A.1. continued.

Planck name	RA	DEC	S_{217}	S_{353}	S_{545}	S_{857}	S_{857}/S_{545}	S_{545}/S_{353}	Note
PG252.29+60.37	170.2222	6.7379	153 ± 33	596 ± 107	1430 ± 228	3089 ± 511	2.16	2.40	G
PG254.17+61.58	171.7317	6.9996	128 ± 35	410 ± 101	1060 ± 240	2348 ± 540	2.21	2.59	
PG231.27+72.22	174.8401	20.4146	90 ± 29	222 ± 68	505 ± 94	585 ± 169	1.16	2.27	L,H
PG280.89+42.43	175.9730	-17.5298	61 ± 28	142 ± 78	519 ± 98	709 ± 209	1.37	3.65	
PG134.01+51.26	176.6610	64.4504	61 ± 29	321 ± 73	1006 ± 160	2504 ± 418	2.49	3.13	
PG245.29+72.50	177.4604	16.9560	92 ± 38	367 ± 88	897 ± 146	1812 ± 326	2.02	2.44	
PG168.15+73.41	177.9516	38.0217	62 ± 29	242 ± 62	686 ± 107	1872 ± 194	2.73	2.84	
PG271.64+62.49	178.9655	3.0522	80 ± 33	237 ± 93	508 ± 152	1274 ± 320	2.51	2.15	
PG250.61+73.51	179.3181	16.4299	95 ± 42	409 ± 137	1232 ± 402	2838 ± 922	2.30	3.02	
PG249.57+74.02	179.5106	16.9908	143 ± 43	854 ± 140	1697 ± 351	3912 ± 734	2.31	1.99	G
PG254.26+73.65	180.1707	15.7903	160 ± 38	833 ± 124	2161 ± 279	5010 ± 634	2.32	2.59	C
PG138.59+62.02	180.5322	53.5779	42 ± 27	168 ± 63	544 ± 94	909 ± 152	1.67	3.24	L
PG251.58+75.04	180.6729	17.2790	150 ± 34	384 ± 79	1072 ± 124	2330 ± 295	2.17	2.79	
PG136.61+60.31	180.9115	55.5297	65 ± 26	103 ± 60	245 ± 86	250 ± 164	1.02	2.38	
PG158.69+75.33	181.9448	38.6075	30 ± 29	208 ± 69	503 ± 86	1127 ± 179	2.24	2.42	
PG143.96+68.94	182.0885	46.3811	88 ± 29	271 ± 59	452 ± 115	673 ± 208	1.49	1.67	
PG124.64+42.47	188.0904	74.5851	78 ± 28	466 ± 68	992 ± 120	2016 ± 250	2.03	2.13	
PG296.90+75.47	191.3130	12.6722	38 ± 33	174 ± 65	394 ± 85	419 ± 164	1.06	2.27	
PG301.66+29.95	191.5511	-32.8997	78 ± 40	216 ± 85	390 ± 109	978 ± 240	2.51	1.80	
PG124.05+68.76	192.2479	48.3583	35 ± 25	128 ± 62	568 ± 95	802 ± 159	1.41	4.45	
PG120.89+69.90	193.8898	47.2046	51 ± 25	106 ± 74	428 ± 92	594 ± 173	1.39	4.05	
PG313.51+81.93	194.4218	19.1962	39 ± 34	257 ± 71	621 ± 117	687 ± 198	1.11	2.42	
PG306.61+59.50	194.7281	-3.3124	82 ± 36	215 ± 82	472 ± 104	1059 ± 178	2.25	2.19	
PG121.98+46.90	194.7768	70.2109	66 ± 23	128 ± 46	364 ± 86	560 ± 145	1.54	2.85	
PG116.56+62.89	197.7940	53.9912	51 ± 26	159 ± 61	426 ± 107	1075 ± 222	2.52	2.67	
PG116.32+62.19	198.1820	54.6603	32 ± 26	111 ± 65	598 ± 106	1337 ± 243	2.24	5.38	
PG084.37+81.06	199.5588	33.9535	48 ± 29	156 ± 78	550 ± 105	697 ± 200	1.27	3.53	
PG323.71+70.55	199.7233	8.8007	27 ± 32	172 ± 74	441 ± 102	890 ± 162	2.02	2.56	
PG007.97+80.28	202.3920	22.7242	73 ± 31	247 ± 70	886 ± 106	1687 ± 183	1.90	3.59	L,C
PG331.60+68.86	202.9291	8.2619	45 ± 34	354 ± 76	793 ± 95	1017 ± 164	1.28	2.24	H
PG104.43+66.26	204.1455	49.2205	50 ± 26	240 ± 59	537 ± 95	946 ± 176	1.76	2.24	L
PG098.67+69.31	204.8089	45.4988	60 ± 29	104 ± 60	323 ± 89	567 ± 181	1.76	3.10	
PG088.65+72.60	205.7301	40.9170	105 ± 34	250 ± 67	485 ± 90	380 ± 179	0.78	1.94	H
PG107.93+46.39	220.5075	67.3860	34 ± 22	197 ± 46	534 ± 87	1008 ± 184	1.89	2.71	
PG081.67+58.67	223.3612	47.5081	55 ± 27	85 ± 57	487 ± 89	758 ± 171	1.56	5.70	H
PG008.90+54.66	225.2252	9.3500	93 ± 40	255 ± 86	719 ± 111	1030 ± 173	1.43	2.82	H
PG045.11+61.10	225.6502	29.3475	72 ± 29	352 ± 70	608 ± 95	829 ± 169	1.37	1.83	L,G,H
PG080.25+49.86	236.1350	50.3961	94 ± 27	220 ± 49	488 ± 92	723 ± 153	1.48	2.22	L,H,C
PG092.49+42.89	242.3240	60.7558	29 ± 23	296 ± 44	800 ± 84	1508 ± 162	1.88	2.70	L,G
PG091.25+39.64	249.2242	60.9445	52 ± 26	313 ± 60	929 ± 138	2551 ± 373	2.75	2.97	
PG067.80+42.08	249.3604	43.0989	79 ± 30	132 ± 75	380 ± 93	447 ± 170	1.18	2.88	
PG090.38+39.23	250.3857	60.4017	160 ± 36	479 ± 119	1540 ± 356	3550 ± 1043	2.31	3.21	G
PG098.24+36.10	253.5277	67.2232	26 ± 19	114 ± 39	306 ± 88	707 ± 168	2.31	2.69	
PG050.24+33.90	257.0167	28.3045	61 ± 31	375 ± 86	906 ± 209	2360 ± 692	2.61	2.42	
PG095.60+33.23	261.6471	65.6767	20 ± 18	153 ± 38	383 ± 91	652 ± 194	1.70	2.51	
PG090.61+32.02	265.0880	61.5781	33 ± 26	167 ± 61	550 ± 105	1329 ± 262	2.41	3.29	
PG066.28+29.27	266.3066	40.5247	45 ± 28	178 ± 59	674 ± 107	1215 ± 226	1.80	3.79	
PG076.11+27.80	270.6847	48.7104	60 ± 23	87 ± 53	471 ± 110	971 ± 214	2.06	5.44	
PG083.31+27.15	273.4877	54.8952	65 ± 25	252 ± 63	553 ± 100	983 ± 179	1.78	2.19	
PG072.75+24.25	274.7849	44.9905	32 ± 24	195 ± 48	524 ± 116	1329 ± 263	2.53	2.69	
PG091.83+23.18	283.8922	61.6503	37 ± 16	254 ± 47	549 ± 98	1332 ± 206	2.43	2.16	

Table A.1. continued.

Planck name	RA	DEC	S_{217}	S_{353}	S_{545}	S_{857}	S_{857}/S_{545}	S_{545}/S_{353}	Note
P G337.39-34.99	306.4514	-59.6130	80 ± 34	134 ± 88	654 ± 192	1615 ± 544	2.47	4.90	
P G014.95-38.34	313.4960	-29.8904	86 ± 36	205 ± 100	830 ± 221	2011 ± 631	2.42	4.05	
P G014.13-44.50	320.4117	-31.6137	74 ± 34	465 ± 99	1378 ± 274	3782 ± 831	2.75	2.96	
P G014.36-44.57	320.5267	-31.4572	127 ± 38	279 ± 119	1063 ± 326	2883 ± 1000	2.71	3.81	G
P G046.00-38.65	322.7808	-7.3297	128 ± 39	303 ± 99	992 ± 215	2724 ± 587	2.75	3.28	
P G053.44-36.27	323.7983	-1.0478	85 ± 34	396 ± 78	835 ± 122	1154 ± 224	1.38	2.11	L,G,C
P G055.15-39.58	327.3209	-1.7852	54 ± 35	228 ± 79	885 ± 130	2379 ± 334	2.69	3.88	
P G054.19-48.48	334.3415	-7.3234	69 ± 33	98 ± 80	426 ± 117	1076 ± 271	2.52	4.33	
P G082.21-32.10	337.0508	19.2092	27 ± 37	210 ± 80	632 ± 178	1474 ± 373	2.33	3.00	
P G019.76-58.75	337.3150	-29.6680	70 ± 30	94 ± 66	397 ± 89	653 ± 157	1.64	4.23	
P G049.33-54.19	337.7131	-12.8720	74 ± 33	274 ± 74	641 ± 106	909 ± 178	1.42	2.34	
P G082.85-32.66	337.8604	19.1018	57 ± 38	254 ± 73	766 ± 103	1850 ± 205	2.42	3.02	
P G060.49-55.29	342.2120	-8.0733	38 ± 34	124 ± 64	714 ± 102	1790 ± 203	2.51	5.76	
P G066.44-52.78	342.5070	-3.7834	151 ± 31	576 ± 92	1767 ± 177	4785 ± 499	2.71	3.07	
P G069.90-55.32	345.7537	-4.0425	70 ± 31	158 ± 70	435 ± 105	921 ± 200	2.12	2.76	
P G074.90-54.52	347.2862	-1.4839	33 ± 27	114 ± 73	530 ± 103	719 ± 229	1.36	4.66	
P G083.73-51.69	349.7349	3.9999	62 ± 30	172 ± 72	806 ± 128	1988 ± 314	2.47	4.68	
P G084.86-52.89	350.9817	3.3882	78 ± 33	357 ± 74	859 ± 145	2155 ± 368	2.51	2.41	
P G091.00-53.65	354.5331	4.6149	52 ± 32	229 ± 73	706 ± 134	1596 ± 311	2.26	3.08	
P G097.78-44.43	354.5638	14.8336	94 ± 33	314 ± 72	994 ± 186	2611 ± 560	2.63	3.16	G
P G041.26-74.44	355.9913	-23.8715	56 ± 29	102 ± 79	446 ± 97	511 ± 165	1.15	4.38	
P G102.83-40.24	356.6420	20.0803	104 ± 35	370 ± 105	1135 ± 242	2728 ± 737	2.40	3.07	
P G087.85-61.51	356.9267	-3.0620	62 ± 32	249 ± 77	594 ± 111	422 ± 236	0.71	2.38	
P G105.01-38.14	357.6658	22.5999	140 ± 37	441 ± 119	1644 ± 306	4516 ± 924	2.75	3.73	

Notes. P stands for PCCS2; all sources except for H G200.61+46.09, which comes from the PHz catalogue, were drawn from this catalogue. Flux densities and errors are in mJy, rounded to 1 mJy. Equatorial coordinates, RA and DEC, J2000, in degrees. L stands for confirmed strongly lensed (Table 1), G for sources included in the *Planck* Galactic cold clump catalogue (Planck Collaboration XXVIII 2016), H for sources included in the *Planck* list of high-redshift source candidates (Planck Collaboration Int. XXXIX 2016), C for sources associated with galaxy clusters (see text), and S for sources with counterparts within 3 arcmin in the SPT catalogue (Everett et al. 2020).

Table A.2. BeeP photometry of candidate strongly lensed galaxies selected at 857 GHz.

Planck name	RA	DEC	SRS	S_{353}	S_{545}	S_{857}	S_{3000}	SN	R_1	R_2	Note
P G126.60-24.47	17.1239	38.2704	6.47	247(+69, −57)	633(+139, −116)	1238(+364, −266)	412(+353, −197)	1.54	1.96	3.01	
P G293.78-69.78	17.4580	-47.0360	5.97	324(+68, −57)	728(+142, −116)	1215(+302, −236)	220(+278, −109)	2.57	1.67	5.53	L,S,C
P G132.16-47.01	19.3765	15.3889	5.10	293(+121, −80)	875(+322, −196)	1892(+890, −498)	480(+613, −237)	1.35	2.16	3.94	
P G138.41-61.22	20.2445	0.7600	5.19	132(+55, −40)	371(+116, −83)	735(+267, −175)	93(+225, −46)	3.40	1.98	7.90	
PE G137.77-41.86	24.5465	19.6534	5.25	107(+59, −34)	296(+156, −76)	591(+400, −163)	129(+360, −64)	1.67	2.00	4.59	
PE G138.84-31.60	28.3941	29.3364	5.04	101(+50, −32)	315(+109, −76)	649(+273, −170)	44(+173, −22)	2.48	2.06	14.70	
PE G299.42-35.45	31.7309	-81.1507	7.41	220(+50, −39)	487(+124, −90)	756(+264, −177)	48(+138, −24)	1.29	1.55	15.68	
PE G145.18-33.98	33.1898	25.3459	5.09	237(+102, −66)	793(+256, −181)	1822(+739, −467)	327(+573, −162)	1.62	2.30	5.58	
P G243.74-69.08	35.1448	-36.0635	6.42	52(+67, −18)	154(+161, −47)	307(+353, −98)	21(+407, −11)	2.27	2.00	14.44	
P G170.56-57.15	36.5264	-3.3135	5.19	108(+68, −34)	224(+135, −62)	311(+237, −89)	7(+81, −4)	2.04	1.39	43.43	
PE G149.41-34.16	36.6416	23.7579	12.01	358(+59, −51)	1030(+149, −118)	1863(+363, −277)	47(+134, −23)	2.03	1.81	39.49	L,G
P G214.55-65.08	40.5677	-25.0993	6.44	146(+53, −40)	503(+124, −97)	1199(+280, −215)	272(+220, −134)	2.91	2.38	4.41	
P G251.10-60.45	44.2520	-41.9078	6.24	169(+66, −47)	505(+155, −106)	1069(+334, −222)	229(+198, −113)	4.73	2.12	4.67	
P G227.77-60.61	46.2943	-30.6084	5.79	155(+89, −46)	395(+175, −96)	647(+316, −166)	18(+144, −9)	3.02	1.64	36.02	L
PE G172.87-43.51	46.7736	5.8185	5.54	279(+122, −80)	911(+339, −209)	2231(+1006, −612)	817(+744, −366)	1.00	2.45	2.73	
P G264.72-52.48	50.5349	-51.9588	5.48	78(+51, −27)	231(+119, −63)	504(+270, −137)	139(+195, −69)	2.07	2.18	3.61	
PE G167.10-28.03	53.8819	20.4359	5.86	298(+111, −76)	915(+294, −199)	2033(+874, −514)	601(+563, −295)	1.40	2.22	3.38	
P G220.47-47.76	59.9835	-24.5896	5.25	93(+45, −28)	347(+113, −80)	840(+291, −194)	104(+200, −52)	1.89	2.42	8.11	C
PE G177.89-28.86	60.2776	13.1428	5.29	327(+145, −90)	959(+406, −232)	2040(+1190, −584)	524(+748, −259)	1.27	2.13	3.89	
P G206.71-38.90	65.1874	-12.2019	6.06	325(+109, −75)	803(+280, −177)	1307(+657, −351)	56(+389, −28)	1.46	1.63	23.33	
PE G227.68-43.36	66.0179	-28.5461	5.27	129(+171, −48)	374(+432, −123)	750(+932, −259)	68(+634, −34)	1.74	2.00	11.09	
PE G274.79-34.59	78.6710	-64.8132	5.18	210(+257, −68)	669(+679, −194)	1445(+1358, −445)	168(+850, −84)	1.24	2.16	8.62	S,G
P G274.15-33.87	80.5288	-64.4013	5.42	189(+92, −55)	530(+228, −137)	1064(+573, −311)	245(+580, −122)	1.43	2.01	4.35	
P G246.88-26.54	89.9582	-40.4288	5.42	223(+63, −48)	856(+171, −138)	2288(+540, −408)	700(+380, −312)	2.37	2.67	3.27	
P G260.64-28.24	91.0354	-52.7328	6.50	153(+47, −38)	489(+118, −86)	1164(+370, −251)	458(+304, −203)	1.96	2.38	2.54	
PE G274.37-29.26	91.2430	-64.8033	7.11	222(+49, −38)	565(+119, −93)	931(+254, −189)	30(+128, −15)	1.27	1.65	30.54	S,G
PE G263.64-27.48	92.9905	-55.2434	6.94	125(+80, −34)	366(+219, −93)	763(+553, −217)	208(+536, −104)	1.19	2.08	3.67	S
PE G242.15-21.80	94.1613	-34.9466	6.65	203(+60, −44)	443(+136, −91)	634(+260, −156)	13(+99, −6)	2.07	1.43	50.46	
PE G273.06-27.78	94.4646	-63.5535	6.64	184(+61, −42)	663(+166, −116)	1683(+464, −323)	488(+351, −226)	1.88	2.54	3.45	
PE G271.27-21.44	107.0614	-60.6701	6.16	137(+57, −37)	406(+149, −96)	839(+376, −222)	124(+254, −62)	1.79	2.07	6.78	
P G177.76+27.63	116.8282	41.7347	5.10	90(+44, −28)	238(+90, −57)	413(+187, −108)	14(+79, −7)	1.13	1.74	28.51	
P G195.00+28.54	122.7289	27.2930	5.57	249(+89, −60)	566(+173, −119)	1010(+344, −236)	363(+325, −180)	2.73	1.78	2.78	
P G207.40+30.68	128.8025	17.8476	5.71	220(+65, −52)	515(+134, −99)	906(+288, −197)	205(+265, −102)	2.73	1.76	4.42	
PE G156.34+36.46	129.5656	60.2823	6.17	154(+57, −40)	522(+151, −103)	1229(+411, −259)	238(+246, −117)	1.38	2.35	5.16	
P G180.36+41.24	135.2606	41.3647	5.79	264(+107, −74)	859(+223, −182)	2019(+523, −417)	751(+584, −373)	2.66	2.35	2.69	
PE G248.44+21.06	139.5978	-18.5756	5.74	219(+51, −41)	662(+117, −95)	1354(+301, −228)	137(+147, −67)	1.57	2.04	9.88	G
PE G248.43+21.23	139.7301	-18.4566	5.99	407(+68, −59)	1249(+146, −130)	2853(+392, −343)	1041(+352, −268)	2.72	2.28	2.74	G
P G174.71+44.71	140.1879	45.4013	5.77	253(+76, −58)	590(+158, −117)	1027(+356, −241)	193(+278, −95)	3.04	1.74	5.32	
PE G250.95+29.95	148.0759	-14.3165	5.05	352(+150, −97)	957(+381, −232)	1963(+918, −502)	749(+675, −368)	1.60	2.05	2.62	
P G241.59+36.89	148.1578	-3.8786	5.72	147(+55, −41)	360(+116, −78)	669(+264, −155)	174(+221, −86)	2.70	1.86	3.84	
P G257.29+26.98	150.0573	-20.3405	6.15	220(+79, −55)	623(+191, −123)	1465(+522, −325)	–	2.88	2.35	–	
PE G266.97+21.81	153.8658	-29.9622	5.24	128(+57, −37)	323(+130, −78)	539(+288, −152)	19(+184, −9)	1.81	1.67	28.65	
PE G269.18+20.78	155.0889	-32.0127	5.07	137(+74, −45)	299(+159, −93)	431(+331, −150)	9(+195, −5)	1.17	1.44	45.61	
P G264.93+26.81	155.6021	-24.8478	5.16	101(+41, −26)	420(+107, −79)	1144(+304, −219)	213(+219, −103)	2.36	2.72	5.38	
PE G257.85+37.17	157.4712	-13.0155	5.29	297(+182, −91)	883(+444, −221)	2295(+1117, −558)	–	1.84	2.60	–	
P G244.31+48.54	158.4228	2.0004	6.00	286(+88, −67)	813(+208, −156)	2011(+604, −430)	–	3.18	2.47	–	
P G256.49+40.45	158.8357	-9.8370	5.52	212(+78, −55)	575(+185, −128)	1270(+471, −288)	–	2.11	2.21	–	
P G257.39+39.85	158.9668	-10.7410	5.53	254(+86, −59)	637(+192, −126)	1384(+439, −286)	–	1.60	2.17	–	
P G232.52+64.41	167.7648	16.4004	5.90	154(+54, −41)	402(+116, −87)	901(+300, −211)	–	3.37	2.24	–	
P G257.23+58.57	170.9027	3.7288	6.70	192(+68, −48)	737(+171, −131)	1960(+517, −382)	598(+349, −278)	2.20	2.66	3.28	
P G134.18+46.86	171.6429	68.3697	5.16	176(+88, −53)	560(+186, −125)	1244(+413, −292)	235(+299, −117)	4.08	2.22	5.29	
P G272.86+47.85	172.8799	-10.3016	5.14	51(+63, −18)	155(+140, −41)	323(+282, −84)	34(+269, −17)	1.86	2.08	9.51	
P G179.18+70.94	173.1686	36.3264	5.66	184(+50, −47)	517(+106, −94)	1324(+294, −234)	–	3.27	2.56	–	

Table A.2. continued.

Planck name	RA	DEC	SRS	S_{353}	S_{545}	S_{857}	S_{3000}	SN	R_1	R_2	Note
P G188.25+73.11	174.5230	32.9658	5.70	87(+32, −25)	225(+65, −51)	468(+161, −111)	–	3.01	2.08	–	L
P G270.56+58.54	176.6579	-0.1922	6.75	273(+69, −54)	590(+133, −101)	1003(+245, −181)	362(+235, −175)	2.80	1.70	2.77	L
P G268.02+66.48	179.5499	7.2905	5.21	128(+60, −37)	330(+131, −79)	582(+244, −143)	44(+123, −22)	3.46	1.77	13.15	H
P G261.42+74.24	182.1263	14.9447	6.23	169(+56, −41)	406(+123, −84)	752(+264, −167)	267(+221, −132)	3.02	1.85	2.82	C
P G287.06+66.90	186.6797	4.7951	6.29	50(+22, −15)	103(+34, −21)	142(+57, −27)	3(+14, −1)	1.74	1.37	49.92	
P G139.00+81.71	190.0659	35.0631	6.60	129(+52, −36)	382(+107, −77)	773(+244, −165)	87(+182, −43)	3.61	2.02	8.93	
P G286.40+83.04	190.7532	20.4464	5.12	171(+70, −48)	450(+162, −113)	787(+376, −224)	37(+156, −19)	1.58	1.75	21.08	
PE G303.39+24.27	193.3978	-38.5955	5.22	152(+69, −43)	591(+214, −142)	1491(+748, −441)	222(+848, −111)	1.29	2.52	6.70	
P G029.94+79.79	204.2273	26.1393	5.05	69(+40, −23)	247(+83, −64)	613(+217, −154)	205(+188, −102)	4.19	2.48	2.99	
P G106.20+61.88	206.0419	53.4993	5.32	144(+52, −36)	402(+115, −83)	732(+242, −166)	30(+124, −15)	3.13	1.82	24.57	
P G052.27+77.90	206.1225	30.5094	6.48	108(+39, −28)	262(+75, −52)	398(+144, −92)	5(+39, −3)	2.51	1.52	74.11	L
P G095.08+61.92	213.1240	50.5943	5.80	137(+47, −34)	339(+104, −69)	628(+223, −138)	147(+136, −71)	4.06	1.86	4.28	
P G112.38+45.80	214.2527	69.5306	5.94	403(+106, −80)	1093(+232, −180)	2115(+498, −378)	412(+480, −204)	6.78	1.93	5.13	
PE G332.22+36.22	217.8552	-20.8954	5.31	114(+81, −38)	319(+217, −91)	627(+523, −204)	82(+389, −41)	1.01	1.97	7.61	
PE G330.84+33.46	218.1387	-23.8648	5.66	88(+45, −28)	273(+95, −63)	581(+214, −134)	78(+132, −38)	1.66	2.13	7.49	
P G010.52+63.13	218.4476	14.6826	5.31	136(+49, −34)	247(+95, −58)	346(+171, −97)	42(+129, −21)	2.31	1.40	8.21	
P G030.03+62.79	222.4941	22.6436	5.11	165(+59, −46)	427(+115, −91)	779(+231, −176)	92(+192, −46)	3.94	1.82	8.51	L,H
PE G341.43+36.23	224.5331	-16.9901	5.46	143(+67, −44)	458(+150, −106)	991(+407, −264)	101(+334, −50)	1.41	2.17	9.84	
P G020.12+51.22	231.7510	13.4125	6.11	212(+89, −58)	477(+179, −112)	742(+340, −202)	40(+270, −20)	1.90	1.56	18.78	
P G008.73+45.18	232.9734	3.8016	5.88	230(+71, −58)	527(+138, −104)	920(+286, −195)	241(+298, −119)	3.13	1.75	3.83	
PE G007.18+42.95	234.1179	1.5931	6.22	158(+47, −38)	422(+96, −75)	813(+226, −157)	154(+146, −76)	1.61	1.92	5.27	C
P G082.93+50.02	234.9139	51.9484	6.14	150(+52, −36)	433(+129, −84)	833(+244, −171)	75(+140, −38)	4.59	1.92	11.07	
P G107.64+36.93	241.8242	73.7842	6.10	229(+60, −48)	576(+133, −103)	1034(+297, −216)	135(+204, −67)	2.42	1.80	7.67	L
P G054.96+40.96	249.8702	33.4433	6.45	154(+42, −34)	364(+83, −65)	632(+178, −132)	103(+127, −51)	2.89	1.74	6.13	
P G099.31+34.06	258.1953	68.5777	5.22	92(+58, −29)	267(+134, −72)	535(+298, −157)	76(+475, −38)	2.29	2.00	7.02	
PE G054.78+20.34	273.0592	27.9778	5.01	252(+92, −69)	702(+229, −167)	1463(+681, −410)	569(+895, −283)	1.36	2.08	2.57	
PE G345.34-22.70	285.8962	-51.4564	5.40	203(+118, −58)	608(+343, −150)	1180(+865, −333)	67(+532, −34)	1.57	1.94	17.55	
PE G336.40-25.51	287.4608	-60.0417	5.25	319(+89, −67)	724(+196, −138)	1285(+450, −290)	442(+467, −218)	1.18	1.77	2.91	
PE G106.16+23.83	291.4330	74.5266	8.40	257(+60, −49)	959(+163, −138)	2528(+545, −425)	828(+357, −281)	2.11	2.64	3.05	
PE G015.04-23.88	297.8042	-25.7533	5.74	208(+63, −48)	522(+150, −102)	948(+344, −215)	144(+247, −71)	1.12	1.82	6.58	
PE G014.87-33.77	308.3849	-28.8693	5.58	94(+59, −31)	239(+136, −65)	415(+315, −126)	21(+140, −11)	1.85	1.74	19.51	
PE G118.33+24.21	316.9182	84.9332	5.71	364(+118, −87)	1230(+333, −253)	2974(+1107, −744)	821(+585, −365)	1.49	2.42	3.62	G
P G004.55-42.72	317.3831	-38.3248	5.23	119(+48, −34)	323(+100, −72)	594(+215, −138)	40(+137, −20)	1.99	1.84	15.04	
PE G046.59-33.70	318.6823	-4.4805	6.55	333(+180, −88)	891(+491, −237)	1618(+1121, −504)	110(+638, −55)	1.02	1.82	14.70	G
PE G056.80-33.20	322.8504	2.9625	5.59	237(+108, −69)	691(+262, −166)	1506(+704, −399)	551(+703, −273)	2.33	2.18	2.73	
PE G079.79-25.18	330.5532	23.1860	5.33	345(+124, −84)	1065(+316, −207)	2923(+972, −616)	–	2.57	2.75	–	
PE G074.81-31.73	331.8080	15.3964	5.96	207(+73, −49)	590(+182, −120)	1516(+559, −346)	–	2.37	2.57	–	
P G332.95-47.82	332.4487	-58.7876	6.29	360(+71, −60)	730(+133, −111)	1179(+264, −205)	399(+297, −193	3.85	1.61	2.96	
P G079.13-35.60	337.2504	14.8849	6.44	84(+34, −25)	212(+80, −50)	453(+215, −116)	–	1.22	2.14	–	
P G058.99-54.74	341.2412	-8.4326	5.18	134(+61, −40)	317(+155, −95)	676(+468, −243)	–	1.58	2.13	–	
PE G095.76-20.92	341.3953	35.2191	5.95	180(+81, −53)	627(+219, −153)	1535(+675, −432)	489(+644, −243)	1.43	2.45	3.14	
PE G079.99-48.54	345.9349	5.1460	5.47	68(+31, −20)	197(+79, −50)	337(+207, −101)	4(+77, −2)	1.42	1.71	95.23	
P G032.65-67.80	348.2116	-25.0753	5.26	97(+38, −30)	269(+81, −61)	662(+215, −151)	–	3.14	2.46	–	
PE G109.34-29.47	358.9165	31.9255	5.52	89(+54, −29)	217(+139, −60)	393(+357, −126)	60(+327, −30)	1.72	1.81	6.51	

Notes. P and PE stand for PCCS2 and PCCS2E, respectively. Units and notes as in Table A.1. The errors were derived from the 97.725% confidence ($\simeq 2\sigma$) upper and lower boundaries of the distributions (S*H2SBU and S*L2SBU), taking the semi-difference between the boundaries and the central values to derive the $\simeq 1\sigma$ errors. SRS stands for SRCSIG, which is a measure of the source detection significance. SN stands for SNRR857, defined as the source average brightness divided by the background standard deviation brightness, $R_1 \equiv S_{857}/S_{545}$, $R_2 \equiv S_{857}/S_{3000}$.

Table A.3. MTXF photometry of candidate strongly lensed galaxies selected at 353 GHz. Units and notes as in Table A.1.

Planck name	RA	DEC	S_{217}	S_{353}	S_{545}	S_{857}	SN_{353}	S_{857}/S_{545}	S_{545}/S_{353}	Note
PG345.90-77.07	1.9719	-36.1645	50 ± 30	202 ± 58	427 ± 110	549 ± 195	3.5	1.29	2.12	H
PG314.57-62.41	3.7358	-53.8762	75 ± 31	287 ± 65	422 ± 89	577 ± 147	4.4	1.37	1.47	
PG123.48-41.23	13.3077	21.6338	66 ± 33	374 ± 89	432 ± 114	942 ± 263	4.2	2.18	1.16	
PG127.01-82.91	13.3958	-20.0593	66 ± 28	255 ± 68	290 ± 115	653 ± 277	3.7	2.25	1.14	
PG297.94-67.76	15.7465	-49.2554	54 ± 28	334 ± 69	294 ± 89	271 ± 156	4.9	0.92	0.88	C
PG215.84-85.99	17.3622	-27.2603	30 ± 32	255 ± 70	322 ± 103	425 ± 223	3.6	1.32	1.26	
PG159.72-82.94	17.3930	-21.4059	46 ± 32	228 ± 72	306 ± 111	626 ± 246	3.2	2.04	1.34	
PG266.70-81.83	18.6412	-33.5940	59 ± 31	243 ± 73	380 ± 113	772 ± 195	3.3	2.03	1.56	
PG159.29-71.93	23.7023	-12.1958	69 ± 35	251 ± 70	540 ± 111	789 ± 197	3.6	1.46	2.15	
PG240.65-74.71	29.0688	-33.2961	60 ± 29	218 ± 71	469 ± 109	892 ± 183	3.1	1.90	2.16	
PG172.24-65.34	31.5870	-9.9270	53 ± 35	263 ± 79	445 ± 101	557 ± 174	3.3	1.25	1.69	H
PG276.79-61.36	32.7061	-51.5447	50 ± 30	205 ± 67	289 ± 90	445 ± 163	3.1	1.54	1.41	
PG262.01-66.10	34.3398	-43.5758	84 ± 27	271 ± 74	537 ± 112	930 ± 211	3.7	1.73	1.98	
PG227.84-69.96	35.4412	-30.4563	54 ± 34	246 ± 66	275 ± 105	429 ± 173	3.7	1.56	1.12	
PG164.17-51.13	37.3518	3.7185	77 ± 39	290 ± 90	253 ± 123	394 ± 221	3.2	1.55	0.88	
PG276.46-54.42	40.9266	-56.5530	75 ± 26	170 ± 55	404 ± 100	592 ± 190	3.1	1.46	2.38	H
PG277.56-53.61	41.1531	-57.5790	66 ± 24	217 ± 47	358 ± 99	523 ± 183	4.6	1.46	1.65	
PG271.53-56.56	41.3713	-53.0432	53 ± 27	302 ± 57	447 ± 126	552 ± 276	5.3	1.24	1.48	S,C
PG284.72-48.56	41.3768	-64.3372	38 ± 22	216 ± 53	343 ± 97	534 ± 184	4.1	1.56	1.59	H
PG223.64-62.24	44.3074	-28.7226	53 ± 33	256 ± 79	431 ± 102	635 ± 186	3.2	1.47	1.68	
PG222.97-60.20	46.5849	-28.2199	54 ± 32	254 ± 81	256 ± 103	404 ± 170	3.1	1.57	1.01	
PG288.74-40.75	49.8876	-72.0458	49 ± 24	236 ± 54	314 ± 129	571 ± 322	4.4	1.82	1.33	
PG194.88-48.95	52.1134	-9.3702	44 ± 34	256 ± 84	667 ± 140	1473 ± 321	3.1	2.21	2.61	
PG222.03-45.79	62.3777	-25.1506	65 ± 35	369 ± 75	631 ± 119	895 ± 185	4.9	1.42	1.71	
PG210.18-41.68	63.6676	-15.7506	79 ± 34	368 ± 80	480 ± 139	424 ± 294	4.6	0.88	1.30	
PG252.28-44.18	66.1880	-46.2626	88 ± 26	250 ± 59	577 ± 107	1313 ± 214	4.2	2.28	2.30	
PG252.72-42.80	68.1375	-46.6978	48 ± 28	172 ± 50	337 ± 101	546 ± 172	3.4	1.62	1.97	
PG239.79-38.25	73.8011	-36.7322	68 ± 28	292 ± 65	488 ± 102	882 ± 201	4.5	1.81	1.67	
PG255.53-38.15	74.9057	-49.0662	72 ± 26	240 ± 54	513 ± 101	822 ± 172	4.5	1.60	2.14	
PG262.35-33.58	82.2573	-54.6265	27 ± 16	218 ± 47	441 ± 121	511 ± 279	4.7	1.16	2.02	S
PG231.49-28.49	83.2327	-27.8126	85 ± 30	284 ± 66	314 ± 93	562 ± 164	4.3	1.79	1.11	
PG246.18-28.94	86.7075	-40.3677	48 ± 25	246 ± 68	699 ± 162	1429 ± 374	3.6	2.04	2.84	G
PG261.72-30.49	87.4899	-53.9363	85 ± 20	291 ± 61	704 ± 163	1497 ± 379	4.8	2.13	2.42	S
PG254.19-27.46	90.7130	-46.9823	101 ± 23	414 ± 81	1229 ± 160	2821 ± 373	5.1	2.29	2.97	
PG159.70+26.61	110.5323	57.3138	95 ± 31	296 ± 69	408 ± 106	554 ± 234	4.3	1.36	1.38	
PG227.04+27.61	133.5962	1.0897	87 ± 29	291 ± 85	270 ± 115	438 ± 233	3.4	1.63	0.93	
PG231.80+31.46	139.0426	-0.4368	75 ± 33	307 ± 68	200 ± 120	373 ± 207	4.5	1.86	0.65	C
PG225.05+40.06	143.6671	8.6510	68 ± 35	307 ± 79	420 ± 107	630 ± 191	3.9	1.50	1.37	
PG188.24+54.14	151.7416	35.9653	105 ± 32	302 ± 64	342 ± 108	566 ± 178	4.7	1.66	1.13	
PG261.11+34.89	158.0973	-16.4464	76 ± 29	324 ± 68	552 ± 118	815 ± 243	4.8	1.48	1.71	C
PG191.21+62.00	161.1758	33.8637	61 ± 30	237 ± 62	533 ± 108	848 ± 173	3.8	1.59	2.25	H
PG143.93+51.40	165.3948	61.0044	21 ± 27	289 ± 54	362 ± 100	550 ± 161	5.3	1.52	1.25	
PG241.50+60.85	167.0309	11.0082	72 ± 30	228 ± 73	285 ± 110	485 ± 205	3.1	1.70	1.25	
PG275.55+36.32	169.3954	-21.5087	37 ± 31	214 ± 65	449 ± 115	633 ± 216	3.3	1.41	2.10	
PG242.20+68.12	173.1852	15.1312	149 ± 34	306 ± 56	717 ± 126	1588 ± 256	5.4	2.22	2.34	G
PG263.55+64.38	176.8315	6.5289	71 ± 34	281 ± 79	651 ± 120	1205 ± 262	3.5	1.85	2.32	G
PG132.62+52.88	179.8096	63.2521	36 ± 27	172 ± 57	258 ± 95	403 ± 180	3.0	1.56	1.50	G
PG251.91+73.87	179.8528	16.4121	72 ± 37	421 ± 110	866 ± 284	1838 ± 579	3.8	2.12	2.06	
PG129.64+47.81	180.4030	68.6606	54 ± 27	214 ± 65	301 ± 96	371 ± 173	3.3	1.23	1.40	C

Table A.3. continued.

Planck name	RA	DEC	S_{217}	S_{353}	S_{545}	S_{857}	SN_{353}	S_{857}/S_{545}	S_{545}/S_{353}	Note
PGC277.03+65.41	182.3533	4.6765	63 ± 34	236 ± 76	227 ± 92	474 ± 168	3.1	2.08	0.96	
PGC143.56+69.33	182.5277	46.1006	45 ± 27	198 ± 66	487 ± 118	574 ± 192	3.0	1.18	2.46	
PGC157.89+76.75	183.3082	37.6623	44 ± 28	237 ± 73	408 ± 113	659 ± 184	3.2	1.61	1.72	
PGC142.49+72.74	185.0319	43.1738	85 ± 26	231 ± 67	398 ± 91	498 ± 156	3.4	1.25	1.72	
PGC125.62+45.73	186.9905	71.2714	43 ± 23	188 ± 51	320 ± 82	641 ± 145	3.7	2.00	1.70	
PGC136.04+72.37	187.3606	44.1924	109 ± 29	279 ± 92	556 ± 215	817 ± 640	3.0	1.47	1.99	
PGC133.50+69.63	187.4790	47.0520	67 ± 27	215 ± 65	356 ± 106	546 ± 181	3.3	1.53	1.66	
PGC124.70+42.41	187.9057	74.6433	100 ± 27	574 ± 62	1122 ± 110	2376 ± 235	9.2	2.12	1.96	G
PGC278.90+81.27	189.1127	19.1145	62 ± 28	305 ± 79	616 ± 151	1031 ± 284	3.9	1.68	2.02	C
PGC296.80+54.40	189.2591	-8.2933	66 ± 37	283 ± 65	259 ± 100	307 ± 180	4.3	1.18	0.92	
PGC122.55+72.74	193.0143	44.3817	26 ± 28	166 ± 54	345 ± 96	424 ± 189	3.1	1.23	2.08	
PGC303.71+49.64	193.3784	-13.2265	127 ± 36	300 ± 99	296 ± 109	546 ± 193	3.0	1.84	0.98	
PGC323.69+78.31	197.1472	16.1371	112 ± 35	281 ± 70	376 ± 104	591 ± 169	4.0	1.57	1.34	
PGC313.31+61.11	197.8533	-1.3524	68 ± 36	595 ± 87	534 ± 113	413 ± 172	6.9	0.77	0.90	C
PGC100.35+78.18	198.5782	37.9210	118 ± 30	197 ± 55	394 ± 98	612 ± 162	3.6	1.55	2.00	
PGC076.26+79.96	201.6254	33.7353	52 ± 27	219 ± 67	328 ± 100	483 ± 181	3.3	1.47	1.50	L
PGC106.61+66.69	202.6467	49.1737	39 ± 25	212 ± 56	325 ± 85	678 ± 158	3.8	2.08	1.53	C
PGC111.34+60.26	203.1017	55.9321	85 ± 26	166 ± 39	270 ± 89	397 ± 179	4.2	1.47	1.63	
PGC007.81+78.02	204.5114	21.5730	93 ± 30	270 ± 76	380 ± 96	595 ± 185	3.6	1.57	1.41	
PGC358.22+75.86	205.0830	18.5710	35 ± 30	228 ± 71	481 ± 107	711 ± 197	3.2	1.48	2.11	
PGC026.55+74.41	209.9023	24.3731	108 ± 27	313 ± 69	467 ± 108	811 ± 187	4.5	1.74	1.49	
PGC010.22+68.85	213.2865	17.5363	36 ± 39	278 ± 80	382 ± 105	574 ± 190	3.5	1.50	1.37	C
PGC060.31+70.00	214.5112	34.6434	95 ± 30	225 ± 62	442 ± 92	631 ± 159	3.6	1.43	1.97	G
PGC090.64+62.63	214.6777	48.6566	41 ± 29	205 ± 53	364 ± 95	612 ± 181	3.9	1.68	1.77	
PGC097.77+58.70	214.8712	53.9103	59 ± 33	212 ± 56	341 ± 92	598 ± 179	3.8	1.75	1.61	
PGC348.16+56.12	216.1829	1.6775	84 ± 38	280 ± 83	402 ± 138	476 ± 211	3.4	1.18	1.44	C
PGC085.35+62.48	217.2119	46.9076	31 ± 28	183 ± 59	287 ± 88	331 ± 198	3.1	1.15	1.57	
PGC071.19+63.27	220.7282	40.9293	90 ± 27	194 ± 61	552 ± 96	757 ± 169	3.2	1.37	2.85	
PGC031.91+64.24	221.2114	23.8177	114 ± 39	317 ± 65	343 ± 116	661 ± 198	4.9	1.93	1.08	
PGC090.99+56.74	221.4609	52.7027	77 ± 29	208 ± 54	327 ± 94	571 ± 176	3.9	1.75	1.57	
PGC057.28+63.02	223.1382	34.9479	61 ± 30	243 ± 67	399 ± 91	588 ± 163	3.6	1.48	1.64	
PGC021.93+57.96	225.9015	17.2454	35 ± 38	282 ± 88	353 ± 137	502 ± 279	3.2	1.42	1.25	
PGC112.46+38.91	226.7890	75.3301	61 ± 25	191 ± 60	522 ± 115	1146 ± 233	3.2	2.20	2.73	
PGC015.04+51.30	230.1174	10.6583	83 ± 39	339 ± 78	437 ± 104	522 ± 179	4.3	1.19	1.29	C
PGC105.01+42.16	232.4433	69.0311	37 ± 19	141 ± 45	461 ± 99	837 ± 173	3.1	1.82	3.27	
PGC100.96+40.40	241.0374	67.5255	32 ± 16	127 ± 42	367 ± 86	658 ± 168	3.0	1.79	2.89	
PGC062.97+43.65	247.2118	39.5797	79 ± 37	462 ± 86	392 ± 102	595 ± 204	5.4	1.52	0.85	C
PGC072.64+41.48	250.0674	46.7262	29 ± 31	492 ± 71	317 ± 99	327 ± 162	6.9	1.03	0.65	C
PGC052.16+36.48	254.5801	30.4520	54 ± 27	223 ± 73	360 ± 101	563 ± 201	3.1	1.56	1.61	
PGC055.60+31.86	260.6126	32.1479	38 ± 28	417 ± 68	271 ± 95	506 ± 176	6.1	1.87	0.65	C
PGC055.86+31.05	261.6050	32.1624	105 ± 29	183 ± 60	310 ± 89	550 ± 211	3.0	1.77	1.70	
PGC086.62+33.71	261.9285	58.1728	54 ± 27	236 ± 45	296 ± 90	532 ± 178	5.2	1.80	1.25	
PGC062.77+27.02	268.1920	36.9959	17 ± 26	208 ± 62	292 ± 103	576 ± 177	3.4	1.97	1.40	
PGC056.55+24.25	269.4627	30.8290	42 ± 34	226 ± 68	593 ± 107	1057 ± 197	3.3	1.78	2.62	
PGC093.25+29.50	270.6105	63.8337	52 ± 16	199 ± 40	450 ± 93	712 ± 159	4.9	1.58	2.27	G
PGC349.67-28.27	295.7143	-48.8606	104 ± 30	400 ± 69	436 ± 107	483 ± 196	5.8	1.11	1.09	
PGC353.03-44.86	320.5751	-46.5724	76 ± 29	196 ± 62	389 ± 106	512 ± 182	3.2	1.32	1.99	
PGC327.56-43.95	329.6385	-64.0109	72 ± 30	257 ± 59	294 ± 91	534 ± 187	4.3	1.82	1.14	
PGC327.39-48.75	338.2416	-61.2784	54 ± 26	265 ± 62	532 ± 86	861 ± 162	4.3	1.62	2.01	S,H
PGC049.13-56.11	339.3857	-13.8882	28 ± 30	265 ± 68	308 ± 103	276 ± 222	3.9	0.90	1.16	
PGC056.96-55.08	340.8430	-9.5821	74 ± 32	256 ± 66	270 ± 102	385 ± 231	3.9	1.43	1.05	C
PGC349.46-59.94	342.2042	-44.5310	59 ± 31	472 ± 65	355 ± 94	268 ± 156	7.3	0.75	0.75	C
PGC351.17-67.38	350.7150	-40.4515	74 ± 34	257 ± 74	289 ± 103	402 ± 167	3.5	1.39	1.12	
PGC325.97-59.46	353.0972	-53.9804	68 ± 27	290 ± 60	542 ± 120	725 ± 229	4.8	1.34	1.87	L,S,C
PGC083.63-69.02	359.5390	-10.3290	325 ± 36	295 ± 53	382 ± 105	470 ± 184	5.6	1.23	1.29	